Fabrication and Characterization of (Au@ Ag) Core-Shell Nanoparticles for Glucose Sensing

Uroosa

Reg.No #00000203334

A thesis submitted in partial fulfillment of requirements

for the Degree of **Master of Science in Physics**

Supervised by

Dr. Faheem Amin

Department of Physics

School of Natural Sciences

National University of Science and Technology (NUST)

H-12, Islamabad, Pakistan

(2021)

FORM TH-4

National University of Sciences & Technology

MS THESIS WORK

We hereby recommend that the dissertation prepared under our supervision by: UROOSA, Regn No. 00000278203 Titled: "**Fabrication and Characterization of (Au@ Ag) Core-Shell Nanoparticles for Glucose Sensing**" accepted in partial fulfillment of the requirements for the award of **MS** degree.

Examination Committee Members

1. Name: DR. SYED RIZWAN HUSSAIN Signature: _____

2. Name: DR. M. ADIL MANSOOR Signature: _____

External Examiner: DR. WAQAS KHALID Signature: _____

Supervisor's Name: DR. FAHEEM AMIN Signature: _____

_____ 11.10.2021
Head of Department Date

COUNTERSINGED

Date: 12.10.2021 _____
Dean/Principal

Dedicating

This Tiny milestone to
My Parents and loving siblings

Acknowledgement

In the name of Allah, the Most Gracious and the Most Merciful, all praises to Allah for giving me the blessing, the chance, potential, and ability to the already existing ocean of knowledge and fulfilling the obligation to explore the universe with the best of my capability.

This dissertation is the result of many people's devotion. Special thanks go to my supervisor, **Dr. Faheem Amin** for all his motivation and support throughout my research work in all possible ways. My experience in **M. Phil** has been amazing and I thank him wholeheartedly, not only for my research work, but also for his patience, motivation, and enthusiasm. my sincere thanks go to the principal of SNS **Prof. Dr. Rashid Farooq** and HOD of physics **Dr. Shahid Iqbal**, for their suggestions and support throughout the program. Thanks to my GEC members **Dr. Syed Rizwan Hussain and Dr. Muhammad Adil Mansoor** for their valuable guidance and encouragement.

Finally, my deepest gratitude goes to my **Parents**, siblings, family, and friends who always prayed for my success. Special thanks to Sadaf Fatima, Ruttab, Sundas, Sabeen and Afsheen for their encouragement, and support.

I also acknowledge **NUST** and all its departments SNS, USPCASE for the facilities and technical support. This is my great pleasure to acknowledge the effort of those whose name may not appear on the cover.

UROOSA

Abstract

Diabetes mellitus affect every organ of human body and is considered as one of the major health diseases. It is very important to continuously monitor glucose level. Nonenzymatic amperometric glucose biosensors based on Gold Silver core-shell nanoparticles were fabricated. Core-shell nanoparticles were synthesized by seed mediated method in which sodium citrate was used as a reducing and capping agent. The shape, surface plasmon resonance effect, optical properties, bond stretching and elemental composition as well as crystalline structure were noticed by using SEM, UV-Vis spectroscopy, RAMAN spectroscopy, FTIR spectroscopy, EDX and XRD techniques. The present work highlights the electrochemical response of glucose concentration by using Gold@ Silver core-shell nanoparticles based upon glassy carbon electrode which ensure the detection of glucose. Furthermore, the selectivity of the sensor against glucose was tested by using ascorbic acid and uric acid. The sensitivity of the fabricated sensors was recorded to be 0.1 µM and 6 µM for (Au@ Ag)20 and (Au@ Ag)2, respectively. The two linear responses of (Au@ Ag)20 and (Au@ Ag)2 from cyclic voltammetry ranging from 0.1mM-0.5 mM and 0.2 mM -0.5 mM and from amperometry ranging from 0.1 µM-14 mM and 6 µM -40 µM were recorded, respectively. The low detection limit, high sensitivity, selectivity, and stability of the fabricated sensor depicts that the sensor can be applied to detect blood glucose as well as noninvasive glucose detection in the body fluid such as sweat and saliva.

Contents

List of Abbreviations

0D	0-dimensional material
1D	1-dimensional material
2D	2-dimensional material
3D	3-dimensional material
XRD	X-Ray diffraction
SEM	Scanning electron microscopy
EDS	Energy Dispersive X-ray spectroscopy
FTIR	Fourier Transformed Infrared Spectroscopy
CV	Cyclic voltammetry
LSV	linear sweep voltammetry
GCE	Glassy Carbon Electrode
Au	Gold
Ag	Silver
NP	Nanoparticles
AuNP	Gold Nanoparticles
AgNP	Silver Nanoparticles
MNPs	Metal Nanoparticles
(Au@ Ag) NP	Gold Core Silver shell nanoparticles
(Au@Ag)2 NP	Gold silver core-shell NPs with gold NPs 2ml plus 1ml of 38.8 mM Sodium tricitrate solution in 30 ml of DI H_2O followed with the addition of 1.2ml AgNO3 aqueous solution(10mM) and 0.4 ml ascorbic acid aqueous (100 mM) respectively.
(Au@Ag)20 NP	Gold silver core-shell NPs with gold NPs 20ml plus 1ml of38.8 mM Sodium tricitrate solution in 30 ml of DI H_2O followed with the addition of 1.2ml AgNO3 aqueous solution(10mM) and 0.4 ml ascorbic acid aqueous (100 mM) respectively.

AA	Ascorbic acid
UA	Uric acid

List of Figures

List of Tables

Chapter 1

1 Introduction to Nanomaterials and Nanotechnology

Nanotechnology is an evolving field that has emerged very rapidly in last few years due to the involvement of new methods and devices for nanomaterial manufacture, classification, and uses. The word ‘nano’ is a Greek word, meaning tiny and the term nanomaterial denotes nanoscale materials that contain internal or surficial nanoscale structures.

1.1 History

The concept of nanoscience began during early 20th century, but the keystone of nanotechnology was introduced in 1959, after a famous lecture of Dr. Richard Feynman at American Physical Society conference entitled "There is plenty of room at the bottom”, where he enlightened scientists about manipulating subatomic particles to generate incredibly tiny structures containing various characteristics and potential particles with one or more dimensions ranging from 1-100 nm called nanoparticles. Nanoparticles having dimensions less than 100 nm can present unusual physiochemical properties, biological and mechanical properties, magnetic, optical, and electronic properties, which are completely different from their bulk form. These unique properties depend on the structure and size, composition and deformities and interfaces of nanoparticles which can all be customized by fabrication [1, 2].

Nanomaterials are the basis of nanotechnology and are expected to open potential approaches for many emerging technological applications such as electrochemistry, photochemistry, and biomedicine. Nanomaterial’s research is quite interdisciplinary since it requires numerous synthetic methods and approaches of characterization. Nanomaterial synthesis plays an important role in application of cutting-edge and focus on the problem of atoms assembling into nanostructured materials intended two coordinating nature, shape, and texture [3].

Typically, two primary methods to the formation of nanoparticles are Top-down method and bottom-up method Figure *1*. Top-down approaches involve the fabrication starting from macroscopic scale to the microscopic scale, while bottom-up approaches develop materials from atomic or molecular scale to the microscale. It also includes a detailed understanding of individual molecular structures, their configurations and complex behaviors, and a broad variety of approaches. Nanoparticles have tremendous potential for developing emerging technologies in a different application in various fields. Nanostructure obtained by Bottom-up approach attain less defects while the nanostructures obtained by top-down approach may contain more defects such as internal stress, contamination as well as surface imperfections.

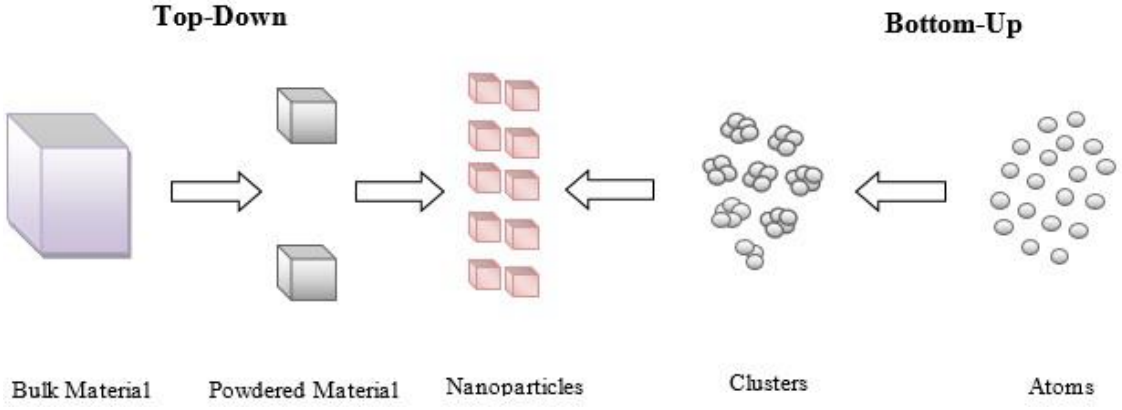

Figure 1: Two synthetic approaches for NPs production [4].

1.2 Classification of Nanomaterials

The term "nano" comes from the Greek word "nanos" which indicate "thin." The term "nano" has been allocated to mean 10^{-9} (1billionth of any unit) [4]. The dimensionality is an important feature that discriminates between different types of nanostructures. Nanomaterials are generally categorized in four groups zero-, one-, two- and three-dimensional nanomaterials (0D,1D,2D,3D) based on their dimensions. This categorization depends on the number of nanomaterial dimensions in the range of nanoscale (< 100 nm).

1.2.1 0D

In 0D nanomaterials, each dimension of materials lies in the nanoscale range (no dimension is >100 nm). Spherical nanoparticles are the most commonly example of zero dimensional nanomaterials.

1.2.2 1D

In 1D nanomaterials, only single dimension is beyond the nanoscale range. Examples of 1D nanomaterials are

- Nanorods
- Nanotubes
- Nanowires

1.2.3 2D

In 1D nanomaterials, 2 dimensions are outside the nanoscale range. Common examples are nanofilm, graphene, nanolayers and nano coatings. This type of materials exhibit plate-like shapes.

1.2.4 3D

This class of materials, no dimension is confined at nanoscale range. Examples of 1D nanomaterials are

- Bulk powders,
- Packets of nanowires
- Dispersions of nanoparticles,
- Nanotubes
- Multi-nanolayers

1.3 Applications of Metal Nanoparticles (MNPs)

Fine MNPs for example Au, Ag, platinum etc. a diverse group of materials with nanometer-sized dimensions are of significant interest. Inherently, an electron's mean free path in a metal at room

temperature is of the range 10−100 nm, and one can expect that peculiar effects will be observed as the metal particle shrinks to this dimension.

1.3.1 Unique Properties of Metal NPs

Two main factors enlarged exposed surface area and quantum effect that be able to change or improve physicochemical properties such as reactivity, strength, and electrical properties. These factors allow nanomaterial properties to vary dramatically from other materials. Concentration of molecules on the surface of NPs is inversely proportional to nanoparticles size. When the size of the particle reduces, a larger number of the atoms are located on the surface in comparison to the volume fraction. Such as 30 nm particle contain five percent of atoms, 10 nm particle contain twenty percent of its atoms, and 3 nm particles contain fifty percent of atoms are on its surface. As a result, small size NPs contain larger surface to volume ratio as compared to larger size NPs. Even though growth as well as catalytic chemical processes occur on the surface, it means that a given mass of material on small nanoparticle is more reactive as compared to the same mass of material on larger nanoparticle.

The captivating qualities of noble metal nanoparticles are strongly influenced by different features such as size, shape, design, crystal structure and texture. The above-mentioned characteristics of noble MNPs have given rise to great capacity for their use in applications, such as pharmaceutical delivery, diagnostic methodologies, summarized in *Figure 2*. Nanoparticles also attract interest in commercial products, particularly in cosmetic products, toothpaste, shampoos, soaps, detergents along with environment monitoring, antibiotic systems, water detoxification, catalysis, etc. due to their superior properties [5].

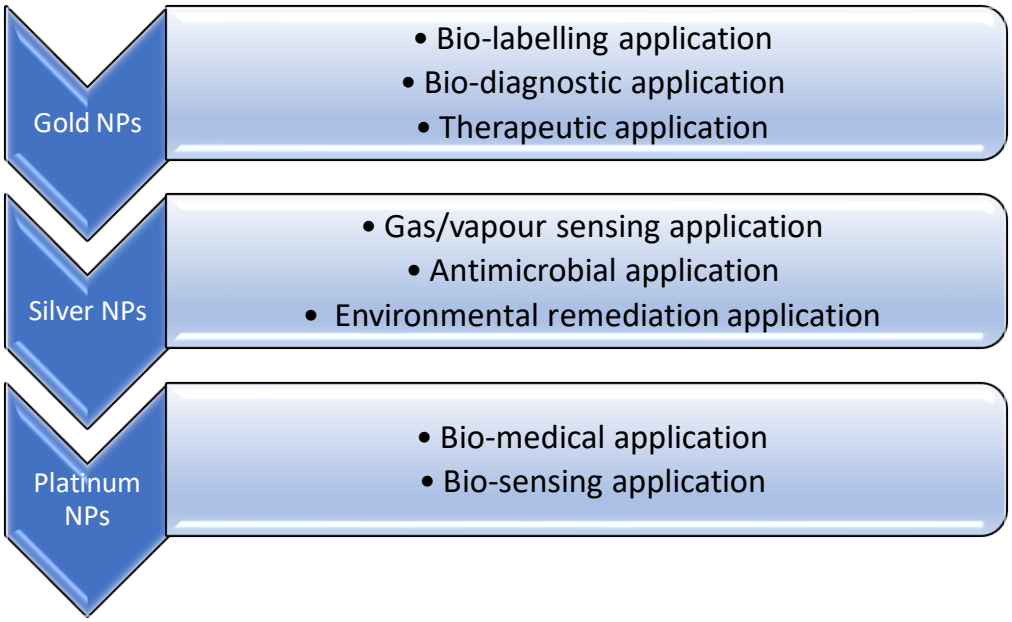

Figure 2: Applications of noble metal NPs.

1.4 Sensing Applications

Nanomaterials are used in various field now including energy storage, water purification, electronics, medicine, concrete, electronics etc. Typically, sensors contain mainly two component parts: a recognition element that provide the target analytes with specific binding as well as a transmitter component to signify the binding activity.

1.4.1 Why to use Gold Nanocomposites in Sensors?

Due to distinct physiochemical attributes, metal nanoparticles have offer excellent platforms for the manufacturing of unique chemical and biological sensing devices.

I. Metal nanoparticles can be prepared easily, and it can be made highly stable.
II. They have distinct optical and electronic properties.
III. They have good biocompatibility with the high surface to volume ratio using suitable ligands.
IV. These properties of metal NPs can be easily adjusted by varying scale, form and the chemical environment that surrounds them.

e.g., the signaling pathway between the recognition factor and the analyte may alter the physicochemical characters of transducer metal NP, including the absorption of plasmon

resonance, conductivity, oxidation/reduction activity, etc., which in turn may generate a measurable response signal to boost analytical performance *Figure 3* . Eventually, metal NPs provide an effective multi-functional platform with a broad variety of organic or biological ligands to selectively bind and detect small molecules and biological targets.

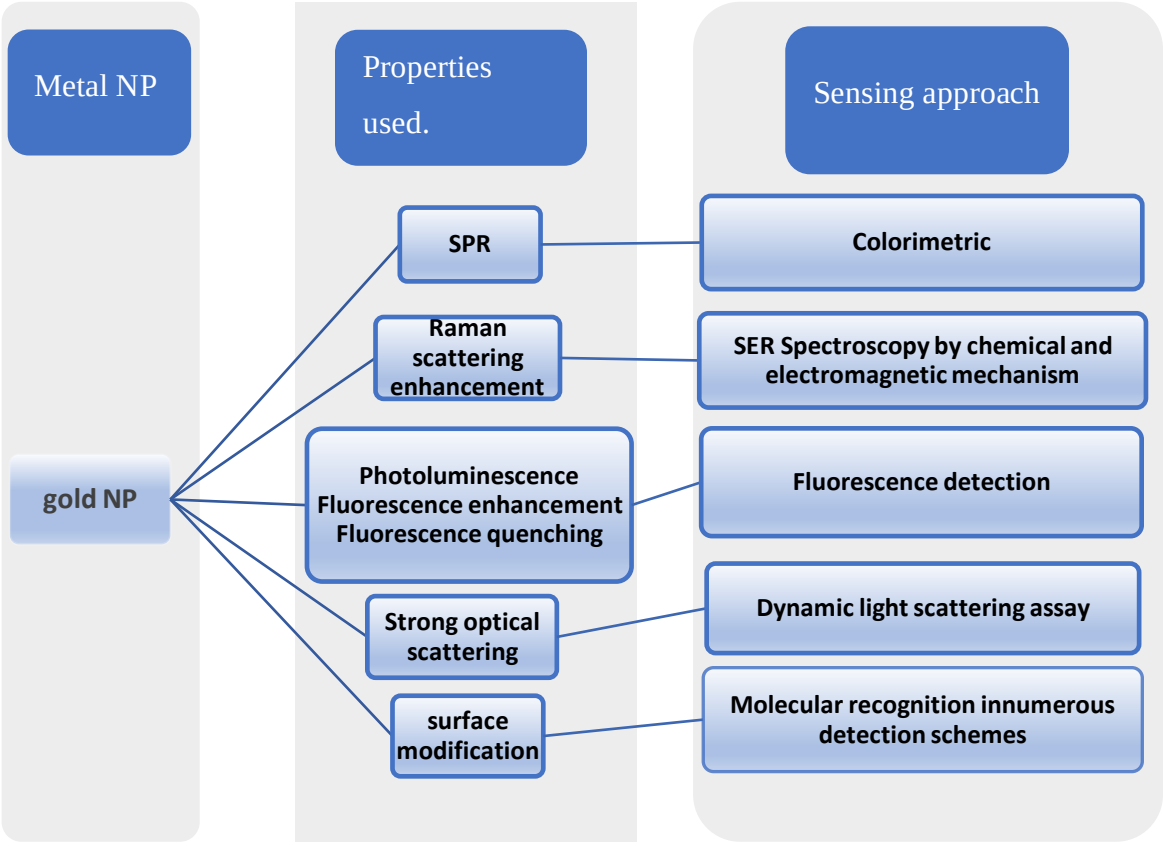

Figure 3: Different properties of MNPs (gold NPs) with unique approaches of sensing [6-8].

1.4.2 Optical Sensors

Metal nanoparticles have many useful photosensitive characteristics that have unraveled the way to novel detecting and imaging methods, providing an extensive variety of sensing strategies including the colorimetric sensing, scattering, surface enhanced Raman Spectroscopy (SERS) and metal enhanced fluorescence (MEF) strategies with very low detection limit (LGL) [9]. Gold NPs have witnessed a keen interest for applications in biological analysis and chemical detection. The SER offers the opportunity to control optical properties of gold nanoparticles by absorbing light at

resonance. This absorption mainly relies on the interaction among the particles as well as on the nanoparticle surface.

1.4.3 Colorimetric Sensors

Colorimetric sensors based on noble MNPs have progressively take more attention. This importance is because of strong localized surface plasmon resonance (SPR) property of noble metal nanoparticles. As compared to other sensors colorimetric sensors provide visible detection and it does not need intricate instrumentation. Colorimetric sensors based on Au NPs are quick, fast, and extremely sensitive, and have been broadly used in on-site real-time monitoring and fast-food quality and safety testing. Developing specific and sensitive metal ion detectors in a solution offer a significant research interest in the analysis of Au nanoparticles [10, 11]. Chen, Yuqing, et al synthesized colorimetric sensor for Cu^{2+} detection base on core -shell (Au@Ag) NPs. Such sensor types are also commonly used to detect mercury lead, and arsenic in water [12] .

1.4.4 Electrochemical Biosensors

Because of low-cost responsiveness, flexibility, and high-speed detection capability, electrical and chemical biosensing in the past couple years has achieved remarkable consideration. Such sensors translate the biological binding events into valuable electrical signals, however the incorporation of AuNPs into these sensors really requires a great deal of work. The attractive features of gold NPs enable them as excellent candidates for improved electrochemical biosensing, such as amplifying the electrode interfaces to stabilize the biomolecules, amplifying the movement of electrons and growing responsiveness.

Chapter 2

2 Literature Review

2.1 Metallic NPs and their Synthesis

Noble metallic nanoparticles, such as Au , Ag, and Platinum NPs, provide great stability, simple chemical fabrication and tunable surface modification [13]. Metal NPs take part in bioactive complexes and chemical detection, involving various sensing methods such as colorimetric, immunoassays as well as Raman spectroscopy.

The following fascinating physiochemical properties of metal nanoparticles make them useful in fabrication of novel chemical and biological sensors.

- Synthesis of metal nanoparticles is straight forward, and simple.
- Offer Unique optoelectronic properties.
- Offer high surface-to-volume ratio.
- Act differently by changing size, shape, and synthesis environmental conditions.

Metal nanoparticles specially gold and silver nanoparticles can be fabricated using different fabrication methods [14] such as chemical, biological and physical techniques as shown in *Figure 4* .

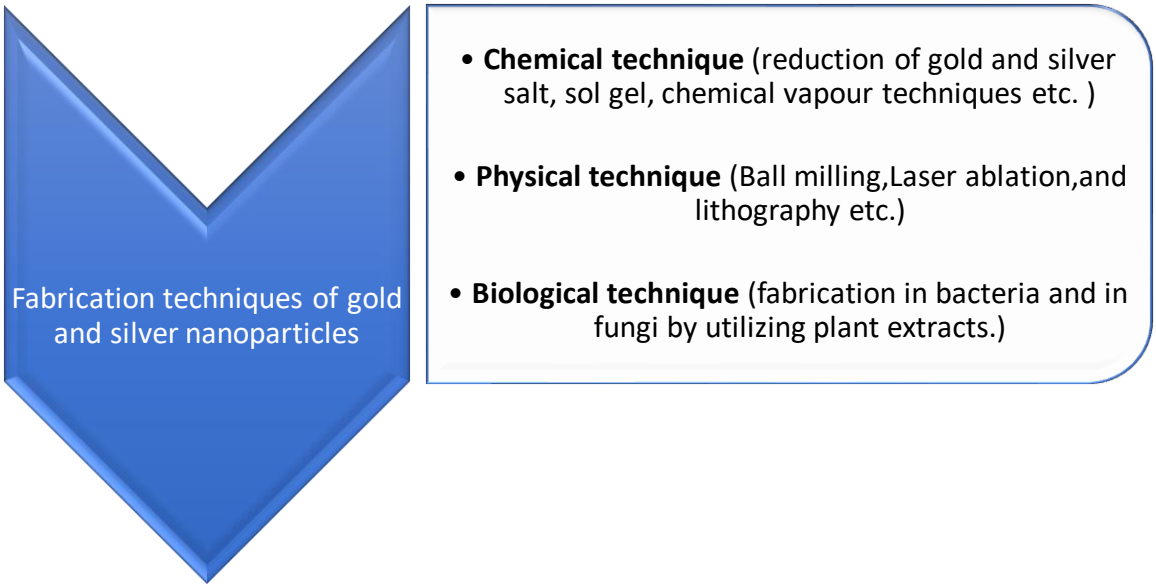

Figure 4: Fabrication techniques for Au and Ag NPs.

2.2 Gold-silver Core-shell NPs

Combination of two metals in a single nanoparticle form Bimetallic nanoparticle. These particles are found in different forms depending upon synthesis conditions such as alloy nanoparticles, core-shell NPs, and cluster in cluster form. They offer extraordinary electrochemical and catalytic behavior. Among them bimetallic Core-shell NPs show enhanced physiochemical characteristics (for example optical, electrical, and catalytic characteristics) compared with mono-metallic nanoparticles due to flexible switchable plasmonic characteristics and highly amplified plasmon resonances caused by cooperative interaction between various metallic mechanisms [15].

Importance of core-shell NP

- Less cytotoxicity
- Cyto and biocompatibility
- Better conjugate with other bioactive molecules
- Increase in dispersibility.

Among core-shell nanoparticles gold and silver are thought to be attractive materials for biomedical sensing and diagnostic applications as shown in *Figure 5* .

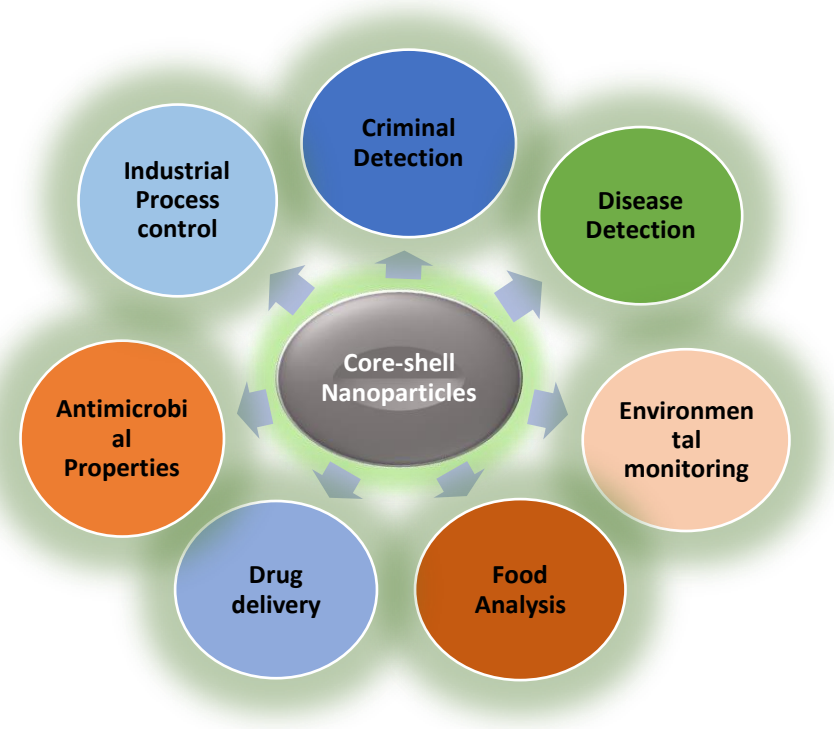

Figure 5: Uses of core-shell nanoparticles.

At the surface of NPs, the oscillations of conduction electrons described optically in the form of surface-enhanced Raman scattering (SPR). AgNPs show excellent responsive SPR compared to AuNPs, but stabilization of these nanoparticles is still a challenge due to its easy oxidation and aggregation [16]. On the other hand gold nanoparticles with good controlled size and structure [17, 18], excellent biocompatibility and stability as well as stronger SPR characteristics are reasonably easy to prepare. Similarly Ag NPs are considered more toxic than gold NPs [19], the toxicity of Ag NPs has been shown by different studies when cells were exposed to Ag NPs. In order to combines the admirable plasmonic sensitivity of silver NPs and chemical stability of AuNPs, bimetallic (gold@ silver) NPs with tunable SPR have been fabricated and broadly utilized in countless applications [20, 21]. Core-shell nanoparticles with different sizes and properties by various approaches reported in the literatures such as gold-Platinum core-shell nanoparticles with improved catalytic behavior were studied by Tan et al [22]. Au-Pd core-shell NPs with enhanced catalytic properties were fabricated and studied by Henning et al [23]. Similarly porous gold-Platinum core-shell NPs were synthesized by Xu, Wenju, et al for Thrombin detection [24].

Different sized (gold@ silver) core-shell NPs were prepared by Selvakannan et al [25] and Tsuji, Masaharu, et al. [26] and Lu et al. [27] by different processes. On the other hand Zhang, Xuehong, et al. [15] developed (gold@ silver) core-shell NPs for colorimetric sensing of cholesterol as well as glucose. While Haili, and Yi He [28] used Dendritic (Au@Ag) bimetallic NPs for glucose sensing. Among unique applications of (Au@Ag) bimetallic core-shell nanoparticles we are focusing to study the electrochemical glucose sensing. Detection application of (Au@Ag) core-shell NPs.

2.2.1 Glucose Sensor

2.2.1.1 Introduction

Glucose is derived from Greek word "sweet." Glucose is a form of sugar with the molecular formula $C_6H_{12}O_6$ used by our body as a source of energy from our diet. Later, it travels through our bloodstream to the whole body known as blood sugar. Hence for regular and normal life activities body get energy from glucose among the most widely distributed materials in human blood.

2.2.1.2 Mechanism of Glucose and Body Response

During travel and break down of food from mouth to intestines glucose is released. Glucose then flows into our bloodstream where insulin helps to deliver glucose into body cells. Our body keeps the level of glucose constant in the blood. Pancreas check and regulate blood sugar level in the body after every few seconds. In case of high glucose level, insulin is released by pancreatic beta cells into the blood. With the help of Insulin, glucose is carried inside muscles and other body cells by acting like a key. In comparison to insulin another hormone called glycogen help in consuming the glucose in the liver. When the blood glucose level drops then alpha cells secrete glycogen, which can be utilize by body when needed. For example, when we have not eaten for a long-time glucose level in our blood drops. The pancreas stops insulin secretion and alpha cells begin to produce glycogen. Glycogen directs the liver to convert stored glycogen and convert it into glucose again. Glucose then travels to our bloodstream to restock the supply until we can feed again. Liver is likewise making its own glucose from the mixture of waste products, fats, and amino acids.

2.2.1.3 Types of Diabetes

High blood glucose level for longer periods of time can damage various body parts by causing problems such as kidney , eye and cardiac failure and low blood flow to lower body parts, weak nerves and immune system as well as slow healing of wound and the likely for exclusion in rare cases. Based on the dependence on insulin diabetes is divided into two types. Type 1 diabetes is insulin dependent and is usually occur in people before thirty years of age, while type 2 is insulin in depend on occurs most frequently in the age after 30 years and in obese people, and consequently affects people in late ages.

2.2.1.3.1 Type 1 Diabetes:

In type 1 diabetes, body is unable to make enough insulin to monitor glucose level. This is due to the reason that immune system bouts and damage cells of the pancreas that make insulin. This is called insulin dependent diabetes because the insulin is injected in the body to make the glucose level constant.

2.2.1.3.2 Type 2 Diabetes:

In type 2 diabetes, the body cells do not react with insulin to utilize glucose for energy. Therefore, the pancreas needs to make progressively more insulin to transfer glucose into the body cells. In the long run, the pancreas is spoiled and becomes unable to secrete sufficient insulin to fulfill the body requirement. *Figure 6* represents the mechanism of type 1 diabetes and type 2 diabetes [29].

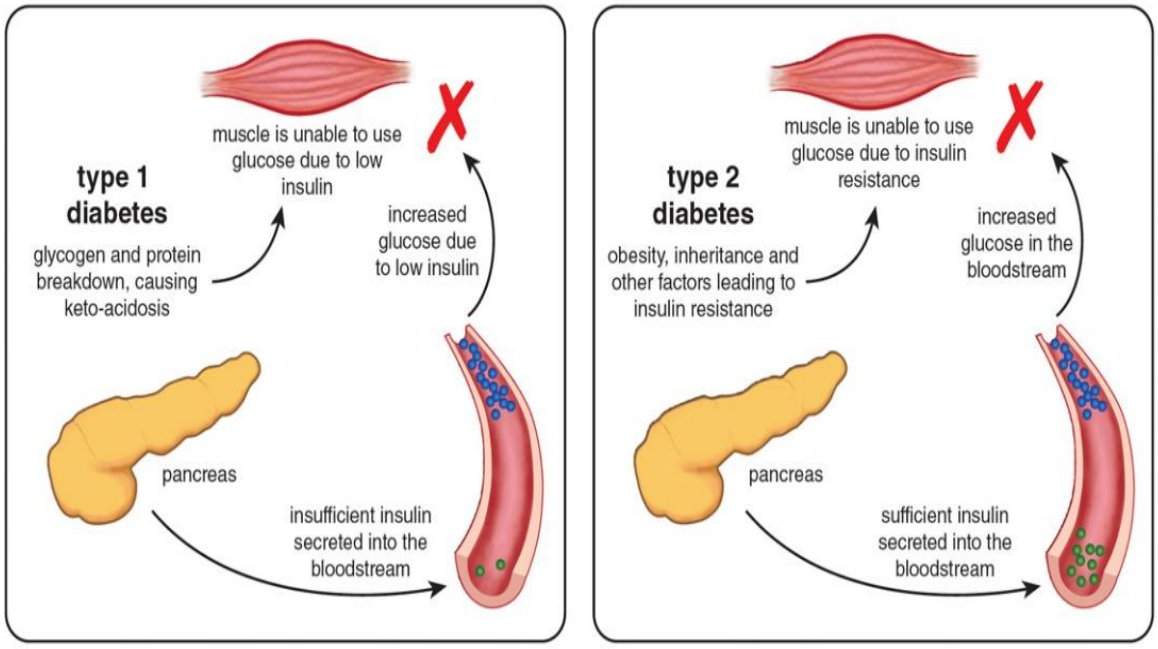

Figure 6: Mechanism of two kinds of diabetes [27].

In case of insufficient insulin, glucose cannot transfer into body parts. In this condition blood glucose remains high this situation called hyperglycemia, a high glucose level means more than two hundred mg/dl, two hours after eating or over one hundred and twenty-five mg/dl fasting. Such high glucose level in the body affects every part of the body leading to different disorders as shown in *Figure 7* . Therefore, continuous monitoring of glucose is required to control diabetes. Different sensing approaches are capable for glucose detection such as colorimetric sensing, optical sensing, and electrochemical sensing.

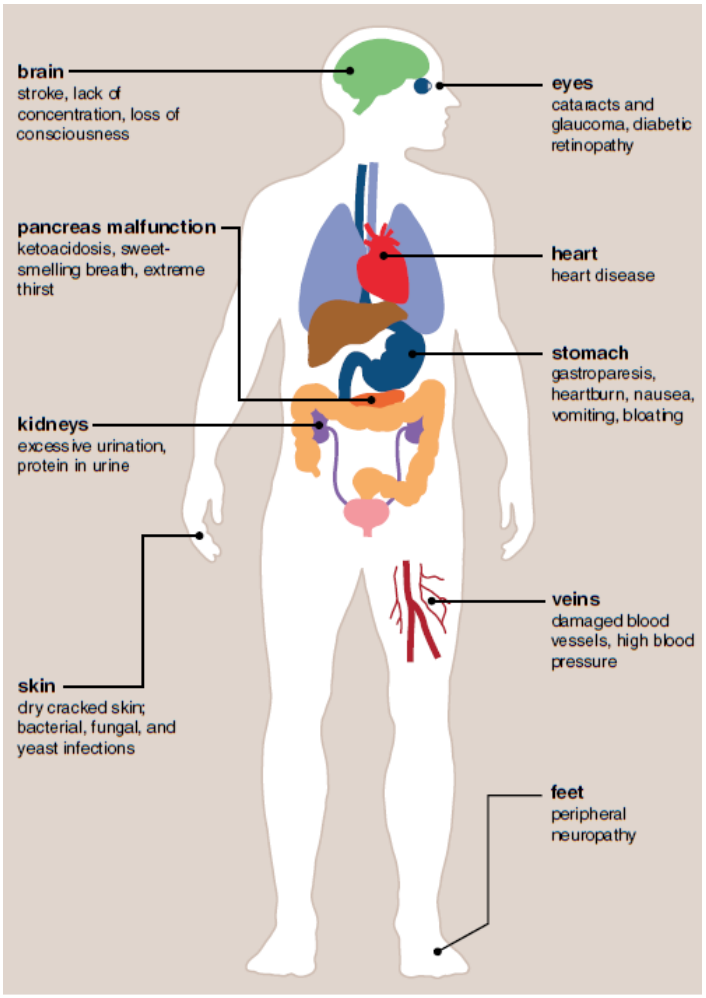

Figure 7: Diabetes effect on human body [29].

In the following section electrochemical glucose sensors and their classification is reviewed.

2.2.2 Classification of Glucose Sensors

Based on electrochemical detection approach glucose sensors are classified mainly into two types.

2.2.2.1 Enzymatic Glucose Sensor

In this type of sensor glucose oxidation occurs in the presence of biological enzyme. When glucose reacts with enzymes usually a glucose oxidase (GOx) which speedup the glucose oxidation and converts it into gluconolactone. This GOx enzyme itself is converted into its reduced form i.e., from its cofactor flavin adenine mononucleotide into flavin adenine dinucleotide ($FAD+2H^{+}+2\ e^{-}$

= $FADH_2$). Based on conversion of enzyme back into oxidized from its reduced form, the biosensors are categorized into three generations *Figure 8*.

In first-generation biosensors, glucose is first decomposed through GOx catalytically which led to the generation of H_2O_2. Later, the oxidation of H_2O_2 occur at the surface of electrode and the current signal is obtained. In this generation oxygen is use as electron acceptor. The major issue with this generation is the error that occurs from the concentration of local oxygen reduction. Clark et al. (1962), developed the first generation of enzymatic sensor, in which they monitored the quantity of oxygen used during the oxidation of glucose or the quantity of hydrogen peroxide produced. They made use of attachment of GOx to a platinum electrode and were able to quantify blood glucose [30].

In the second-generation biosensors, artificial electron mediators were used to address the oxygen limitation. These mediator such as hydroquinone(HQ), ferrocene, and numerous redox organic dyes were employed among GOx and the electrode in order to make the transfer of electron rapidly [31]. This affects the interference problem produced by unstable dispersed O_2 and very high-level capability of hydrogen peroxide(H_2O_2). Additionally that it also reduces the sensor's sensitivity toward interfering elements because for the reduced mediator, oxidation occurs at a low potential [32]. Some problems concerned with mediator-based sensors are low stability and loss of mediator due to its toxic effect.

In third-generation biosensors, the GOx is directly linked to the working electrode which enables the transfer of electron directly and produces output signal. This was achieved by integrating enzyme with metal and semiconductor which also accelerated the reaction rate. Krishnan et al used seed mediated method to fabricate Pd@ Pt core-shell nanostructured glucose biosensor by promoting direct electron transfer between enzyme and electrode [33]. The polymer(chitosan) was first decorated on Pd@ Pt core–shell and then glucose oxidase was attached to the particles by covalent bond. The sensitivity of the sensor was recorded as 6.82 $\mu A\ cm^{-2}\ mM^{-1}$.

In all these processes the electrons from the glucose oxidation reaction are initially taken up by enzyme and then delivered to oxygen in first generation or to mediator in second generation or to

the electrode immediately in third generation. The inherent instability of enzymes and the limitation of oxygen in glucose checking strips are two major challenges for glucose sensors. Therefore, advancement in glucose sensors was desired which introduces non-enzymatic glucose sensors.

2.2.2.2 Non-enzymatic Glucose Sensor

Nonenzymatic glucose sensors are those which involve the direct electrochemical oxidation of glucose ($C_6H_{12}O_6$) to gluconolactone ($C_6H_{10}O_6$) in the absence of biological enzymes. This electro-oxidation of glucose occurs at nanostructured electrodes such as metal nanoparticles [34].Core-shell nano-structures that have high surface area and offer high electrocatalytic activity may prove to be excellent sensors. Furthermore, these electrodes offer high sensitivity, stability, low cost as well as simple and easy construction.

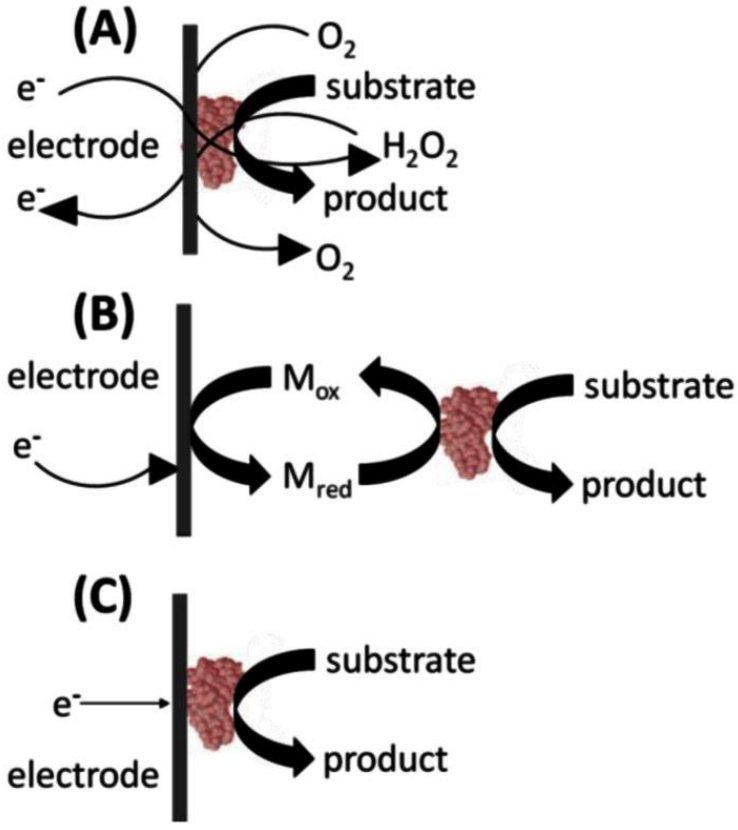

Figure 8: Enzymatic glucose sensors generations [35].

With the regular advancement of fabrication techniques, it has been realized that the size, shape, and other characteristics of some nanomaterials can be controlled and lead to advancement in their selectivity, sensitivity, and efficiency.

Preidel et al. used platinum electrode surface for direct oxidation of glucose without any enzyme. This electrocatalytic glucose sensor was used for long term glucose detection about more than 2.5 months. The sensor was used for in vivo glucose detection by inserting into sheep's artery but the main problems were low sensitivity due to clotting on electrode surface and long sensor running time [32].

Similarly, Pt-based non-enzymatic and amperometric glucose sensors were developed, but also exhibit certain problems, for example high cost and low selectivity and kinetics [35-38]. Core-shell nanomaterials take more importance toward sensing field due to their diverse composition and size and shape control properties to reduce the cost and enhance the catalytic action of the non-enzymatic glucose sensor. The present work is basically involving the uses of bimetallic core-shell NPs for glucose sensing.

Mei, He, et al. [36] created a non-enzymatic glucose sensing method involving Co@Pt nanoparticles. Under optimized conditions the sensor revealed excellent electrocatalytic action and stability for glucose sensing with 0.3 mM LDL. Yang, Xuejuan, et al through seed mediated method [37] developed gold@silver core-shell nanorods for glucose detection with 0.67 μM detection limit. Chen, Xianlan, et al. developed non-enzymatic glucose detector involving Au@Pd core–shell flower shaped nanostructures with 1.0 nM detection limit [38]. Similarly, Shim, Kyubin, et al. (2019) developed a non-enzymatic glucose detector involving Au@ Pd core–shell NPs, and then with the incorporation of gold NPs into the platinum shells to fabricate nanochannels. The detection limit towards glucose was recorded to be 445.7 (±10.3) nM [39].

In the present work, an electrochemical non-enzymatic glucose biosensor involving Au @Ag core-shell nanoparticles have been developed. (Au@Ag) core-shell nanoparticles with different core ratios have been synthesized by seed mediated method previously reported in literatures [40, 41] *Figure 9*. XRD, UV-vis spectroscopy, SEM FTIR and Raman spectroscopy were employed to

characterize (Au@Ag) core-shell bimetallic nanoparticles. By cyclic volumetry as well as amperometry the performance of glucose biosensor was examined. Furthermore, for the selectivity and performance of the obtained glucose sensor the important operational parameters were examined in detail.

Figure 9: Graphic representation of (Au@Ag) core-shell NPs [43].

Chapter 3

3 Fabrication and Characterization Techniques

Different characterization and synthesis techniques with their working principles have been discussed in this chapter. It includes X-Ray Diffraction (XRD), Scanning electron microscopy (SEM), Energy-dispersive x-ray spectroscopy (EDX), ultraviolet and visible spectrometer (UV-Vis Spectroscopy), Fourier transform infrared spectroscopy (FTIR) and Electrochemical sensing. Similarly in the other part of this chapter fabrication technique for (Au@Ag) bimetallic core-shell nanostructure is discussed.

3.1 Fabrication Technique

Different steps are required to synthesize required samples. In this section we will discuss various chemicals, fabrication steps and fabrication apparatus for the fabrication of gold silver colloids and (Au@Ag) bimetallic core-shell nanoparticles.

3.1.1 Chemicals

- Chloroauric acid ($HAuCl_4$ 1 wt.%)
- Sodium citrate ($Na(cit)_3$)
- Deionized water (DI)
- Silver nitrate ($AgNO_3$)
- Ascorbic acid ($C_6H_8O_6$)

3.1.2 Apparatus

- Beakers
- Weight balance
- Hotplate
- Pipette
- Petri dish
- Stirrer

3.1.3 Fabrication of Gold Colloids

Sodium citrate thermal reduction process was used in fabrication of gold colloids. Following steps were followed during this process.

- 90 ml of DI water was kept at 100°C in a beaker on hot plate, to boil.
- 1ml of 1 wt.% gold salt aqueous solution ($HAuCl_4$) was put into above solution at constant stirring.
- Two ml of 38.8 mM sodium citrate aqueous solution was put into the above solution stir constantly for 45s.
- When the color of the solution appeared purple red, it was kept in refrigerator to cool down quickly ***Figure 10.***

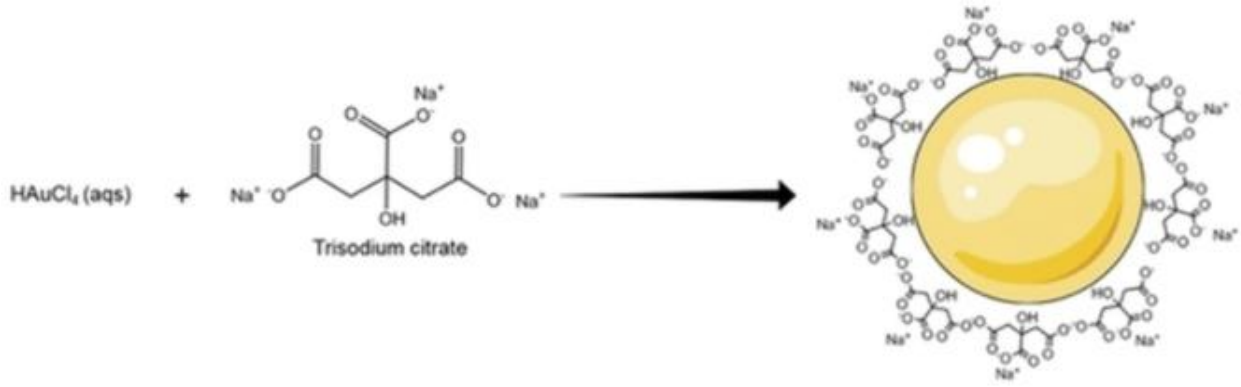

Figure 10 Graphical representation of AuNPs formation by means of trisodium citrate as a reducing and capping agent [42].

3.1.4 Fabrication of (Au@ Ag) core-shell NPs

The core shell bimetallic NPs were fabricated by means of seed mediated method. Following steps were followed in seed colloid technique.

- Two samples of 30 ml DI were taken followed by addition of the prepared gold colloids 2ml and 20ml, respectively.
- One ml of 38.8 mM trisodium citrate solution was put into each solution at constant stirring.
- 1.2 ml of 10 mM $AgNO_3$ aqueous solution was put into each solution at constant stirring.

- 0.4 ml of hundred mM ascorbic acid (AA) aqueous solution was also added up further to the prepared solutions at constant stirring. After 14 hours the mixture was washed with DI water by centrifugation for 15 minutes at 12,000 rpm. Hence core-shell NPs were obtained.

3.1.5 Synthesis of Glucose Solution

The prepared bimetallic NPs were then tried for glucose detection. The required chemicals and applied procedure that were followed are given below.

3.1.5.1 Chemicals

Deionized water (DI), sodium hydroxide (NaOH), (Au@Ag) core-shell NPs, glucose ($C_6H_{12}O_6.H_2O$), Ascorbic acid (AA), Uric acid (UA), Glassy carbon electrode (GCE) and ethanol.

3.1.5.2 Apparatus

- Hotplate
- Beakers
- Centrifuge tube
- Micropipette

3.1.5.3 Synthesis Methods

The electrode used for sensing purpose was Glassy Carbon Electrode (GCE). GCE was cleaned through using polishing kits.

Core-shell NPs were deposited on the GCE by drop cast method. The GCE was then dried by leaving it overnight. Other solutions required for sensing and selectivity are 0.1M NaOH,0.1 µM-14mM glucose and 50 µM AA and 50 µM UA.

3.2 Characterization Techniques

Characterization techniques play an essential role to examine the overall properties of material. Specific characterization techniques along with their working principles that have been used in this work are given below.

3.2.1 XRD

This technique was used to study the crystallographic properties of the prepared bimetallic NPs. XRD gives valuable information about the material or thin film such as crystalline phase and orientation, size, and shape, density, and grain identification.

- **Principle and working**

In this technique X-rays is focus on the material and the intensities and scattering angles leaving the material is measure. It works on the principles of Bragg's law, as when incident light is diffracted by a 3D array of molecules, atoms, or ions *Figure 11*. In 1913 Bragg summarized this behavior by giving the expression below.

$n\lambda = 2d\ Sin\Theta$

Where λ=beam wavelength

n=integer

Θ=angle between incident ray and surface of crystal

d=spacing between the diffracting planes

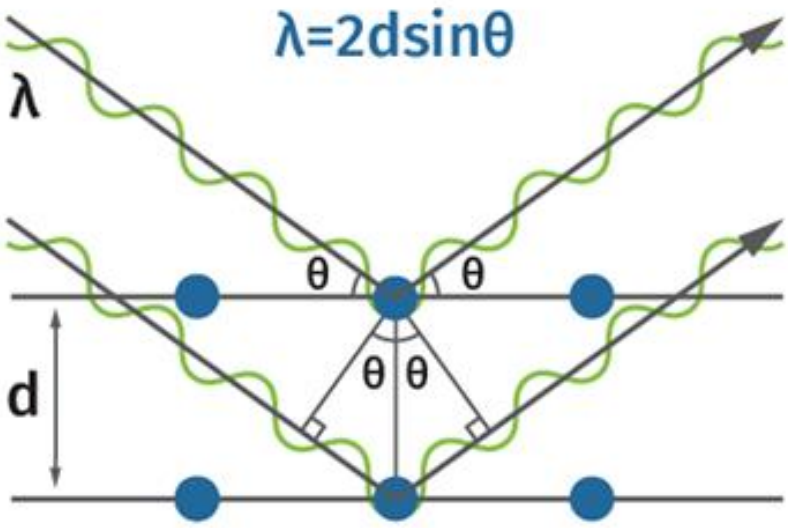

Figure 11 Principle of XRD.

Depending on the value of n the waves either add up or cancel each other by constructive and destructive interferences.

In case of constructive interference, the result is recorded and plotted between intensity and 2Ɵ. 2Ɵ is the totality of the incident and reflected angles. Furthermore, X-ray diffraction displays result from electromagnetic waves impinging on a regular pattern of scatters. X rays are utilized for diffraction pattern production because its wavelength is of the same order as the spacing between the planes of crystal.

3.2.2 SEM

In this technique high energy electron beam is used for sample investigation. Image is obtained by the interaction of atoms of sample and electron beam occur. These atoms contain information about topography, composition, and crystal structural information about the sample.

- **Working Principle and Construction**

High energy electron beam is focused on the specimen, the resulted signals are then assembled and examined to form image. These signals carry information about chemical composition, topology as well as crystallography about the sample surface.

Different components of SEM and their working for chemical analysis are given below in *Figure 12.*

- **Electron Column**

Electron column is the main source of electron. It is cylindrical in shape fitted above the specimen chamber. This chamber is kept under vacuum to allow electron to flow in the chamber easily and interact with the sample. Depending on the condition and choice, the magnitude and acceleration of electrons can be adjusted. The electron column further consists of lenses, scan coils, condenser, and objective aperture. The force with which electron hits the specimen depends on the voltage which accelerate these electrons. Mostly between2-30kV voltage is used.

- **Magnetic Lenses**

It consists of two electromagnetic lenses: condenser lens and objective lenses. Through these electromagnetic lenses fine concentrated beam like probe is produced which scans and magnify

the specific area of the specimen. When current passes through winding sets, produces magnetic field among windings. The electron then passes through magnetic field obeying Lorentz force.

- **Specimen Chamber**

This chamber is located below the electron column where sample is placed for analysis. The chamber contains holder, air locks, stage, CCD camera as well as detector where sample is placed in vacuum at 10^{-3} Pascal pressure. The sample is degassed and dried to remove contamination and water before placing it in the chamber. Some coating (gold/carbon) of the sample is done in case of non-conducting sample.

- **Detectors**

Detectors play an important role to detect and make detailed image of the sample. The signal from the sample is received by detector and converted into signal after further processing, which in turn is converted into SEM image and then further into energy dispersive X-ray spectrum.

In short, all the sensors collect and analyze the sample signal, which contain backscattered and secondary electrons.

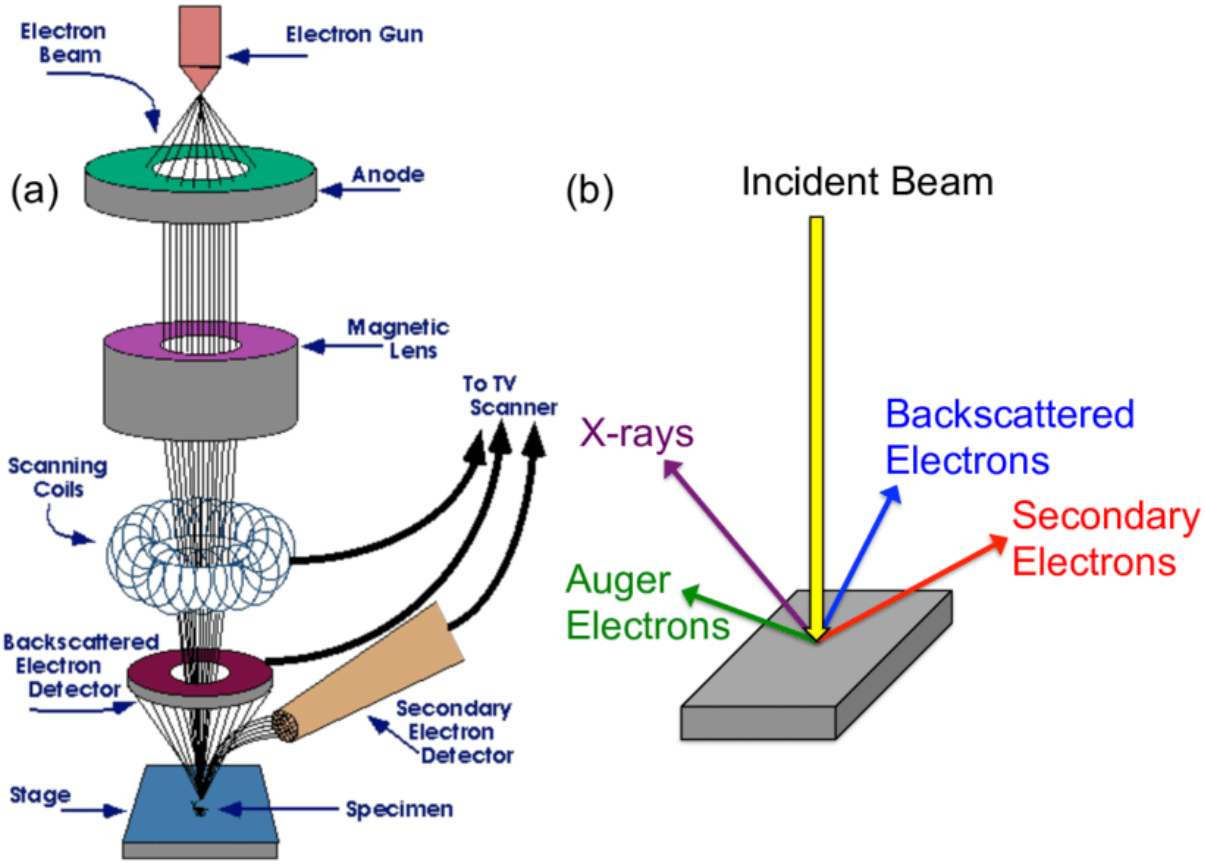

Figure 12 Components of SEM [44]

3.2.3 EDS

EDS is an analytical technique use to examine material elemental composition and chemistry. This technique is associated to electron microscopy based upon x rays' creation that exposes the existence of elements in sample. This device relies upon the analysis of a sample through interactions between electrons and matter. When highly energetic electron hits the material atoms, different types of X-Rays are emitted. These emitted rays then give useful information about the different structures of elements which are the basic principle of EDS.

- **Principle and Working**

Highly energetic electron beam is focused on the sample. This interaction will create characteristic X-ray because atom has different energy states, so electrons are excited from lower energy states

to higher energy states of the atoms by creating vacancies in inner shell. The vacancy fills when an atom returns to ground state. As a result, a specific amount of energy emits. This emitted energy is equal to the variance between 2 energy levels; one is shell contributing the electron and other is vacant shell. This emitted X-ray give energy. Each element has different energy levels and generates X-ray, whose energy is characteristic of that element. In K, L and M shell, no two elements have same energy value.

In energy X-ray spectroscopy, the characteristic X-ray are measured by the detection equipment. Semiconductor detector is used to detect the X-ray and then convert it into current which is caused by electron hole pair in semiconductor. Analyze spectrum of high energy verses intensity display on a computer screen. In electron microscope, backscattered electrons produce image of a sample's topography. Using EDX, the percentage of weight is determined present in the element of the given sample.

3.2.4 UV-Vis

This technique is also known as electronic spectroscopy due to transition between electronic energy-levels of molecules due to absorption of visible or ultraviolet radiation. In this spectrometer when light of specific wavelength is passed through the sample either it is absorbed or fully transmitted. The light should be in visible electromagnetic range (190nm-400nm) and ultraviolet (400nm-800nm). The result gives important structural information about the absorbing atoms or molecules.

- **Principle**

Large amount of incident radiation is absorbed if greater number of absorbing molecules are present in a sample. Resultantly, it leads toward high peak intensity obtained in absorption spectrum. This work on the principle of Lambert-Beer law ,according to this law the amount of incident radiations absorbed is directly related to the amount of absorbing molecules and path in the absorbing medium through which radiation pass [43].

This law is mathematically express as:

$$\boldsymbol{A} = \varepsilon \times \boldsymbol{c} \times \boldsymbol{l}$$

here

- **A** is absorbance
- **Ɛ** is molar extinction coefficient ($dm^3\ mol^{-1}\ cm^{-1}$)
- **c** is concentration of solution ($mol\ dm^{-3}$)
- ***l*** is optical path length (cm)

- ## Components and working of UV-Vis.

The components of UV-Vis include: a radiation source, which covers wavelength range from 200 to 1100 nm; monochromator; prism; filter or grating to separate continuum source into individual or selected range of wavelength; a sample holder or cuvette; a detector and readout device. Absorbing substance is taken diluted because only small numbers of absorbing molecules are needed for detection. Two compartments are used in the dual beam spectroscopy. One compartment contains a reference sample in which the sample material is not added and other is sample under test. First, the reference sample is exposed to ultra-violet and visible light and the amount of the rays adsorbed are examined. Then the light passes from the test sample from which some light reflects, and some absorb. In case of light absorption, the electron jumps to a higher orbit and makes the transition. The detector measures the wavelength of light. The reference beam without sample interaction travels to detector from light source. Energy is absorbed, when electron is excited to higher molecular orbital by emitted wavelength which corresponds to energy-level. The ratio between beam intensities of reference and sample ($I_\circ/I$) is recorded by detector. From intensities large gap the UV absorbance spectrum is prepared by computer and plot highest UV light absorbance wavelength *Figure 13* [44]. The radiation is separated by monochromatic, or diffraction grating and then passes through the sample containing in pure silica or Pyrex glass cuvette. The remaining transmitted beam intensity difference come from reference and the sample is then detected by photomultiplier, photodiode, or semiconductor to convert information into electric signal which is then readout in the form of spectrum.

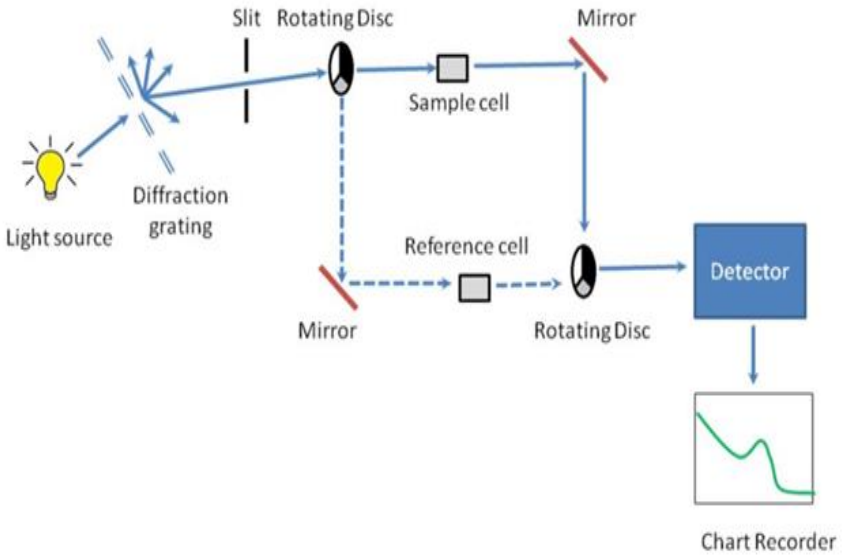

Figure 13: UV-visible spectrophotometer schematic diagram, describing optical properties of sample [43].

3.2.5 FTIR

This analyzing technique measure the infrared region (IR) of electromagnetic radiation when subjected to infrared radiations. The infrared region has longer wavelength and shorter frequency as compared to visible light, the range of IR10,000 cm^{-1} to 100 cm^{-1} and 4000cm^{-1} to 400cm^{-1} . This technique analyzes the chemical groups in the material.

- **Principle and Working**

The infrared radiation is passed from the sample and causes vibrational transitions when absorbed by the molecule. These vibrations are then studied to examine the molecular composition and structure of materials. The infrared radiation is produced by radiant black-body source and is passed into interferometer in which encoding of spectral take place. Interferogram is produced because of destructive and constructive interference from different path lengths recombination of beams. The beam then passes into the sample compartment where the energy of specific frequencies is absorbed by sample. The detector is used to quantify the signal of for the entire frequencies (Energy/Time). A reference is provided for operation of instrument by superimposed beam at the meantime. At the end, the interferogram spontaneously subtract the background

spectrum from the sample spectrum to obtain desirable spectrum, by Fourier-transformation computer software ***Figure 14*** [45].

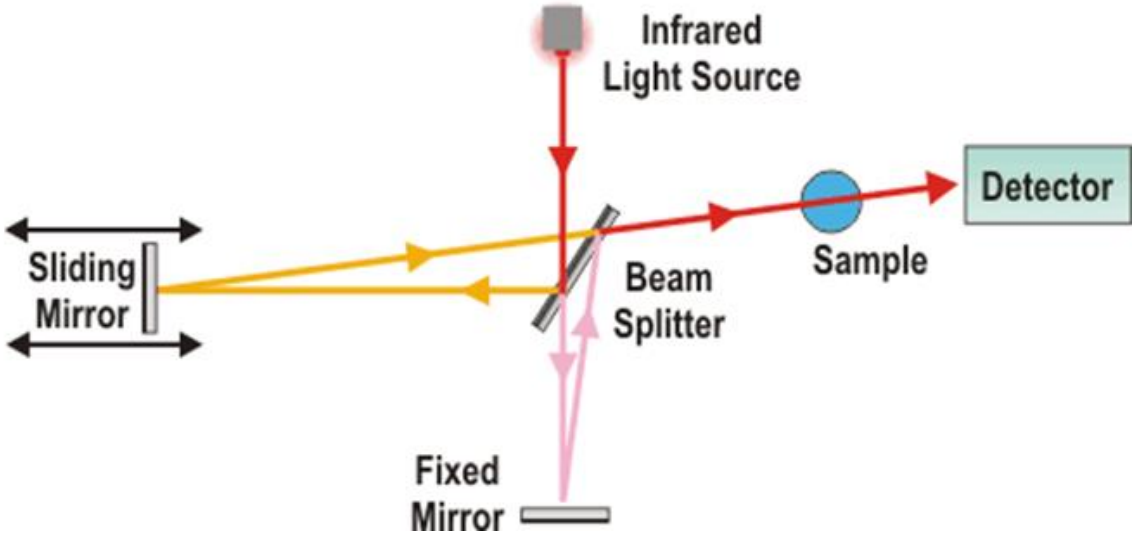

Figure 14: FTIR- spectroscopy, an analytical technique.

3.2.6 Raman Spectroscopy (RS)

This technique was first time discovered in 1928 by C.V Raman. He uncovered the fact that scattering of light occur when radiation of light falls on the sample.

- **Principle and Working**

When monochromatic light interacts with sample molecules (gas, liquid or solid) it may either be reflected, absorbed, or scattered from the sample ***Figure 15*****.** The scattering of molecules gives structural information about the molecular structure of the sample. Rayleigh scattering occurs when ν of the incident and scattered light from the sample is same. This scattering does not give useful information about the sample and is termed as elastic scattering. On the other hand, when the wavelengths of the incident and scattered light mismatch, then scattering occur at different frequencies as compared to the frequency of the incident photon. This effect is called Raman Effect or inelastic scattering. Approximately 1 out of 10 million photons scatter inelastically.

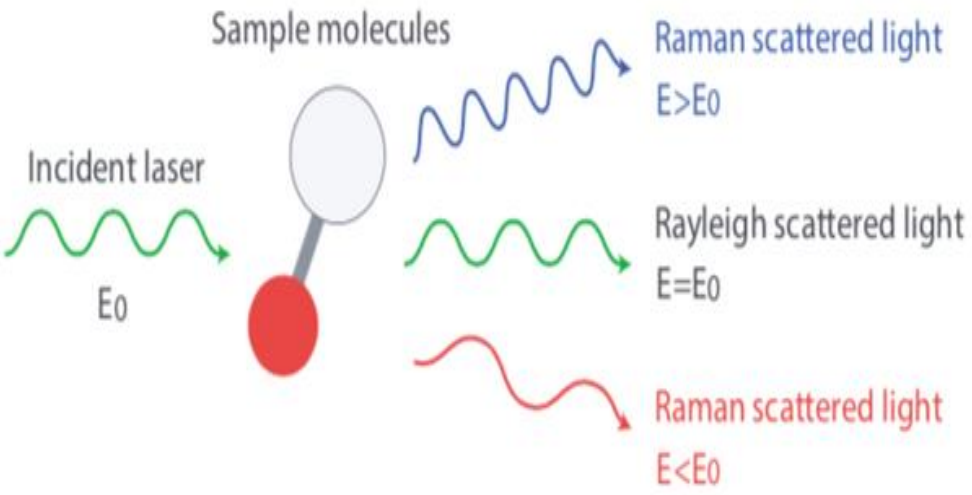

Figure 15: Principle of Raman scattering.

Raman analysis gives following information about the sample.

- Chemical structure and uniqueness
- Polymorphic behavior and Phase details
- Intrinsic stress strain and impurity

In short it is a chemical fingerprint that gives frequent details about similarities and differences of the samples.

3.2.7 Potentiostat

Potentiostat is derived from word potential. It is an electronic device used to measure electrochemical response of the active material from oxidation and reduction mechanism. It consists of three electrode system and work on the principle of controlling voltage differences amount between working and reference electrodes and then calculating the flow of current between counter and working electrode.

- **Construction**

Potentiostat consist of six different clips with different colors. Their setup consists of following connections. The working and counter sense assemblies relate to working and counter electrodes which are further connected to active electrode material using GCE and platinum wire, respectively. AgCl electrode is normally reference or auxiliary electrode and the ground clip is left

open, or it is connected to faraday shield table and figure. The function of working electrode is to be carried out the electrochemical reaction. Voltage difference is controlled by reference electrode which is taken as reference point as compared to other electrodes in electrochemical setup. The electrical circuit is completed by counter electrode which quantity the current when the flow of electrons occur between working and counter electrodes [46]. Potentiate characterizes many techniques but here we will discuss cyclic voltammetry, linear sweep voltammetry and amperometry.

3.2.7.1 Cyclic Voltammetry (CV)

This technique is an electrochemical method that measure the reaction kinetics of electron loses or gain occurring in the material.

- **Principle**

The electrode is put in some solution of known molarity and the current flow is determined by adjusting one electrode's potential and seeing the voltage needed to pass the electron between the electrode and the molecule of interest. These two electrodes are attached to a potentiostat to control the voltage between two electrodes. The law which governs it is ohmic law.

- **Working**

In CV at fix rate the sweeping of the control voltage occurs two values of the voltage. The resulting voltammogram show the behavior of the electrochemical reaction occur at electrode surface. The resulting current vary with change in voltage and scan rate as shown in ***Figure 16*** .The voltammogram may have oxidation and reduction peaks but the amount of kinetics at electrode surface can change the number of peaks. In case of forward sweep the reactant are converted into products but in reversed scan the product of electrolyte converting gradually into reactants back. In backward sweep the current flow from the electrolyte to electrode back but the behavior of both can be explained in the same manner.

The put-on potential regulates the redox species at the electrode surface. This behavior is described by Nernst equation.

$$\boldsymbol{E = E_0 - (T/nF)\ ln\ (Ox/Re)}$$

In the above equation

- E = electrochemical cell
- E_0 = standard reduction potential
- R = molar gas constant
- T = absolute temperature
- n and F are the total number of electron transfer and Faraday constant.
- ***Ox and Re* =** Relative activities of the oxidized and reduced analyte at equilibrium.

The distinct attributes of voltammogram for a reversible electrochemical response is shown in *Figure 16* .Voltage partition between the current and positions peaks remain constant as the scan rate changes, the ratio of the peak currents is equal to one. The peak currents are equall to the square root of the scan rate [47].

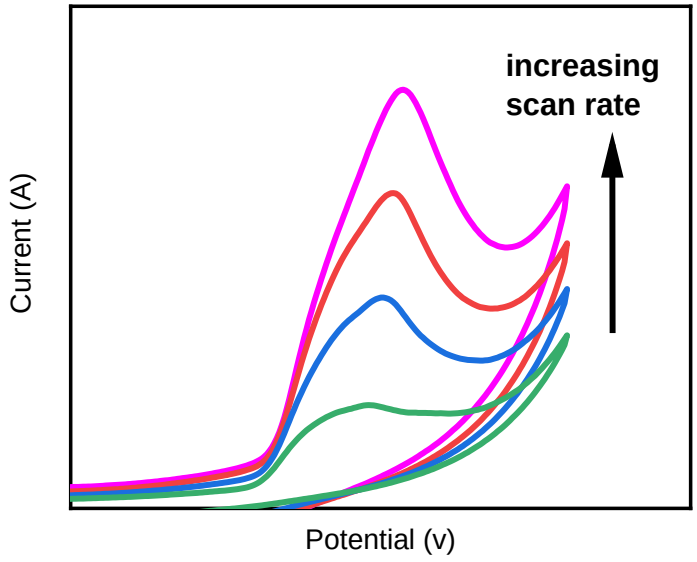

Figure 16 CV Voltammogram of (Au@ Ag)2.

3.2.7.2 Linear Sweep Voltammetry (LSV)

In LSV, potential across the working and reference electrodes is linearly swept in a time and current is recorded. The species oxidation or reduction action is indicated form the peak in the linear signal. However, the setup of electrode for both LSV and CV are same. The factor on which LSV depend are:

- The number of the electron transfer reaction in a specific time.
- The amount of electron transmission
- The chemical responsiveness of the species
- Voltage scan rate

At the beginning when linear sweep voltammetry starts from the left side there is zero current, but it increases as the voltage increases till peak before dropping down ***Figure 17***.The current in LSV begins to flow and there are variations in the surface reactants. The peak in LSV occurs when the diffusion layer has expanded adequately above the electrode at some point of the electrode and the Nernst equation is not fulfilled by the flux of the Nernst equation and current starts to fall.

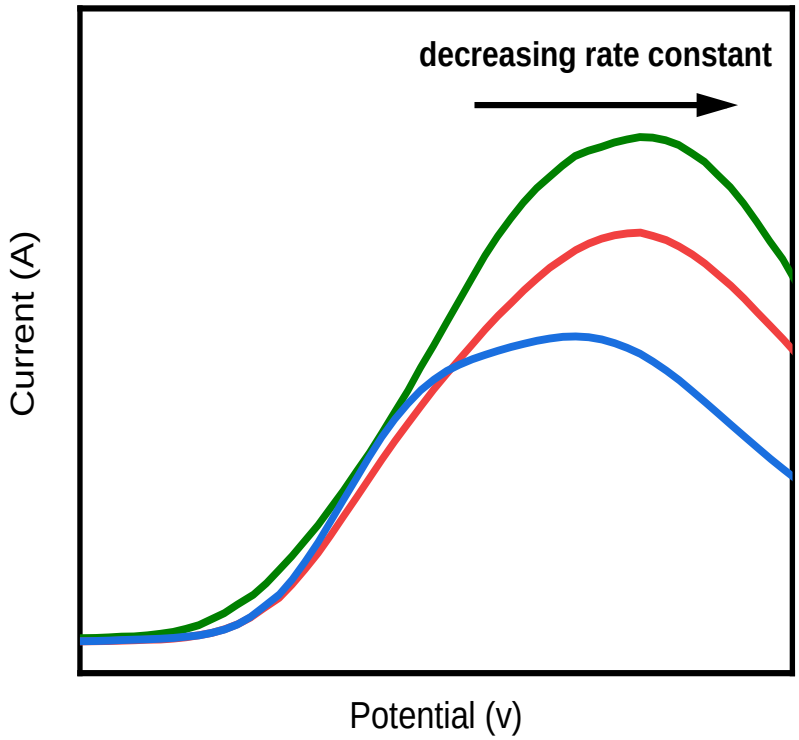

Figure 17 Linear sweep volumetry of (Au@ Ag)2.

3.2.7.3 Amperometry

Amperometry is the electrochemical method where current is measure as a function of time by applying constant potential to working electrode. The term “amperometry” is therefore originated from the “ampere” current measuring unit and the “meter” measurement device used in this technique. L. C. Clark (1956) developed first amperometric sensors for sensing of dissolve O_2 in blood. Since the potential remain unchanged all over the experiment, no charging currents are produced. Therefore, the amount of analyte electrolyzed according to Faraday's law (Q = nNF) is given by direct integration of the sensed currents. The strength of the measured current is generally directly related to the strength of the material being reduced or oxidized; therefore, this method

can be used for different testing applications. This approach provides the ability to selectively differentiate between a variety of electroactive species in solutions by judiciously selecting the potential applied and choosing the electrode material.

Chapter 4

4 Results and Discussion

4.1 XRD

To investigate the crystal structure of the prepared spherical gold @silver bimetallic core-shell nanoparticles were described with X-Ray Diffraction. The XRD patterns of AuNPs seed and (Au@Ag) core-shell NPs are displayed below. Each pattern shows four diffraction peaks ranged from 35º to 70º that were attributed to diffraction of FCC structure of metallic (Au and Ag). Moreover, the peaks of the prepared NPs demonstrated a shift from pure gold to silver structure. This result indicated that core-shell nanoparticles were successfully prepared.

4.1.1 XRD of gold Nano seeds (AuNPs)

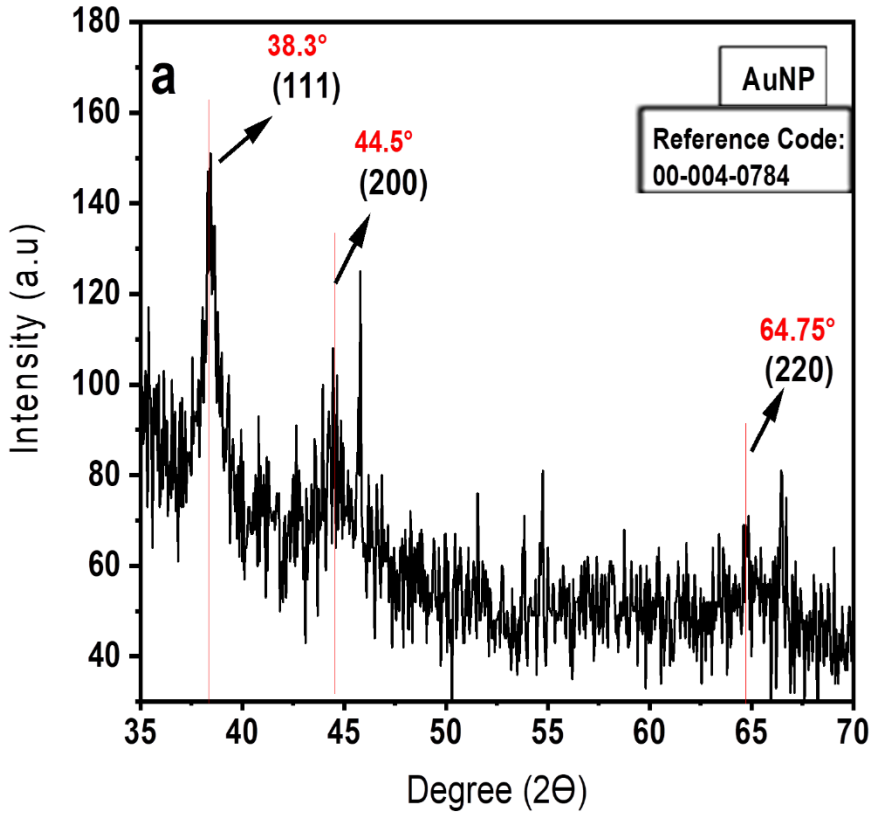

Figure 18: XRD pattern of AuNPs.

Figure 18 show XRD pattern of Au colloid solution prepared by citrate reduction method. The diffraction peaks appear at 2Θ = 38.3,44.5 and 64.75 matches with reference code (Ref.Code 00-004-0784), corresponding to miller indices (111), (200) and (220). This result attribute to the FCC structure of gold.

4.1.2 XRD of (Au @Ag) core-shell NPs

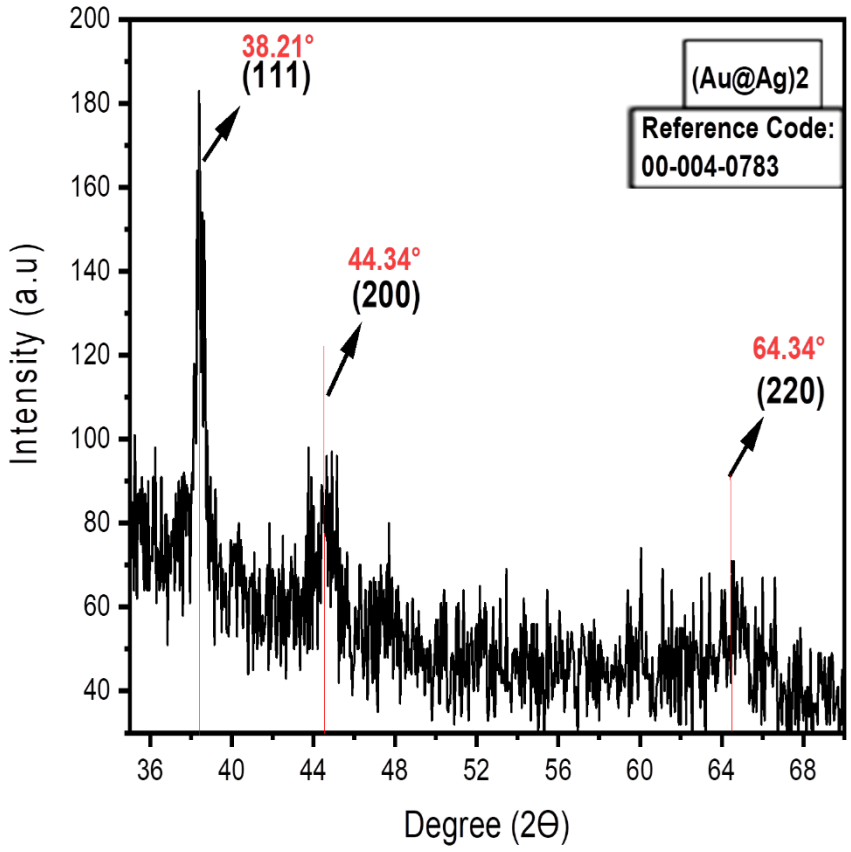

Figure 19: X-Ray Diffraction pattern of (Au@Ag)2 NPs.

Figure 19 shows XRD diffraction pattern of bimetallic (Au@Ag)2 NPs. The core-shell nanoparticles were prepared by seed mediated method with 2ml of Au seed. XRD of (Au@Ag)2 NPS shows the diffraction peaks at 2Θ = 38.21, 44.34 and 64.34 which matches with the reference code of silver (Ref.Code 00-004-0783), corresponding to miller indices (111), (200) and (220). This confirms the Ag shell formation by complete reduction of silver ions and deposition on the surface of Au NPs.

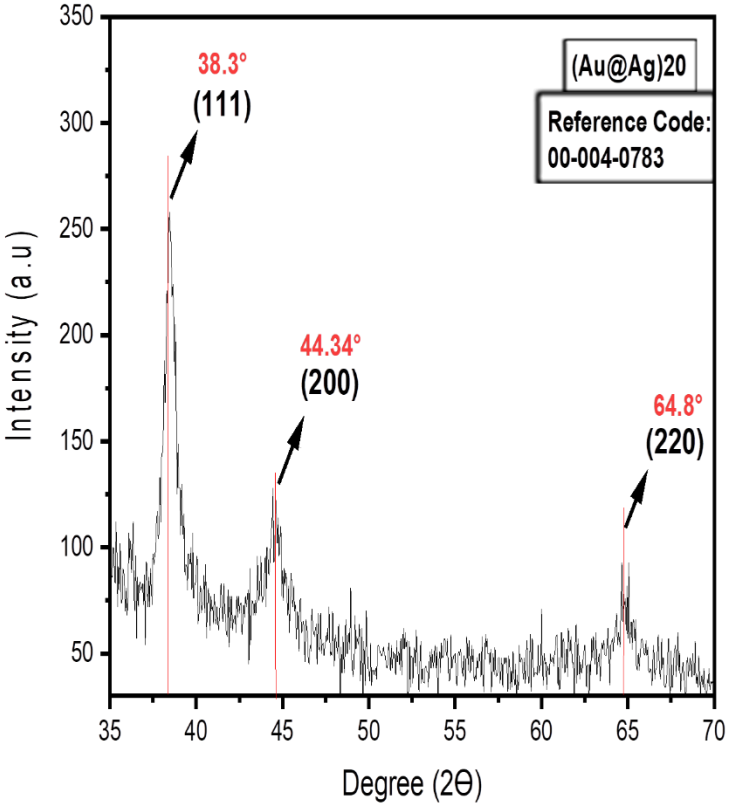

Figure 20:X-Ray Diffraction pattern of (Au@ Ag)20 NPs.

Figure 20 shows XRD of gold silver core shell bimetallic (Au@Ag)20 NPs. the diffraction peaks at 2Θ = 38.3, 44.34 and 64.8 matches with reference code of silver (Ref.Code 00-004-0783), corresponding to miller indices (111), (200) and (220). This confirms the Ag shell formation by complete reduction of Ag salt.

XRD results show that with the higher concentration of gold, corresponding to Au (111) a distinguished increase in the peak strength occurs. This indicates that due to growth in grain size an improvement in crystallinity of gold also occurs. The growth in grain size offers more chances to plane arrangement in symmetric pattern which in turn enhances the crystallinity as well as constructive interference. These results show that (Au@Ag) core-shell NPs are successfully formed and shows a highly crystalline phase [41].

4.2 UV-Visible Spectroscopy (UV-Vis)

4.2.1 UV-Vis of Gold NPs

SPR is photosensitive effect in which the collective oscillations of free electrons occur with the same frequency of coming light. shows the SPR peak of AuNPs. These NPs were produced by using trisodium citrate as reducing and stabilizing agent which was added quickly. By the addition of trisodium citrate, reduction of Au salt occur that changes the solution transparent. When nucleation and growth occur the solution, color alters into wine red from light yellow. This change in color confirms gold NPs formation. At 520 nm the SPR spectrum was observed demonstrating Au seed formation [48].

4.2.2 UV-Visible of (Au@ Ag) core-shell NPs

Figure 21 shows SPR peaks (Au@Ag) core shell bimetallic NPs synthesized with varying gold core. Gold and Silver NPs were first produced by reduction method then bimetallic NPs were produced by seed mediated method, then the core size were changed by changing gold quantity to study various bimetallic NPs, while maintaining all other reaction circumstances constant. The Au seed contain absorbance band at 520 nm while for the bimetallic NPs, the plasmon peaks appear at 403 nm and 412 nm, respectively. This can be completely ascribed to plasmon resonance of silver particles as shell. The presence of 1 absorbance band matching to AgNPs specifies that bimetallic core-shell NPs formed homogeneously rather than the formation of independent particles [49, 50]. Hence from UV-Vis absorbance spectra we can conclude that only Ag ion reduce on the surface of gold core, instead of forming Ag nucleation sites, and results bimetallic core–shell nanostructure.

In case of bimetallic nanoparticles, a red shift of the plasmon peak remarked gradually as the seed volume was reduced from 20 ml to 2 ml, indicating large sized particle formation. The particles size increases because in case of less number of Au seed particles the adsorbed Ag ions per particles increase and after reduction of silver ions the thickness of the shell increases [40, 51].

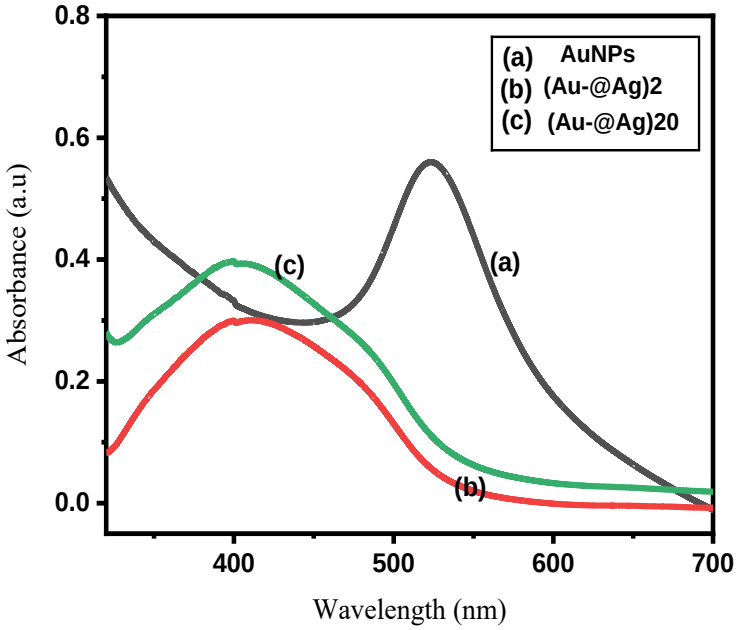

Figure 21 UV-visible absorbance band of (a)AuNPs seed and (b and c) (Au@Ag) core-shell NPs with changed gold seed volume:(b) 2ml, (c) 20ml.

4.3 SEM

The SEM analysis of (Au@Ag) core-shell nanoparticles is presented below.

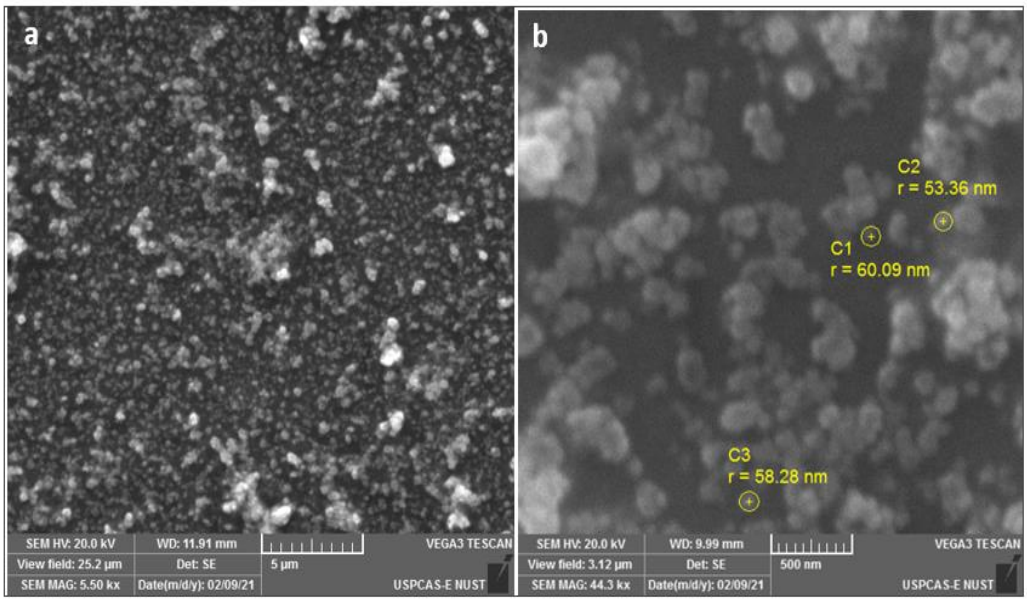

Figure 22 SEM results of (Au@Ag)2 at (a) 5 µm and (b) 500nm, respectively.

Figure 22 illustrations SEM images of (Au@Ag)2 NPs made, but small size spherical particles can also be noticed straightforwardly with average particle size of r =57.2 nm. The EDX (table) results of (Au@Ag) NPs synthesized by seed mediated method shows elemental configuration of Au=0.32% and Ag =1.86% which approves the core-shell NPs creation.

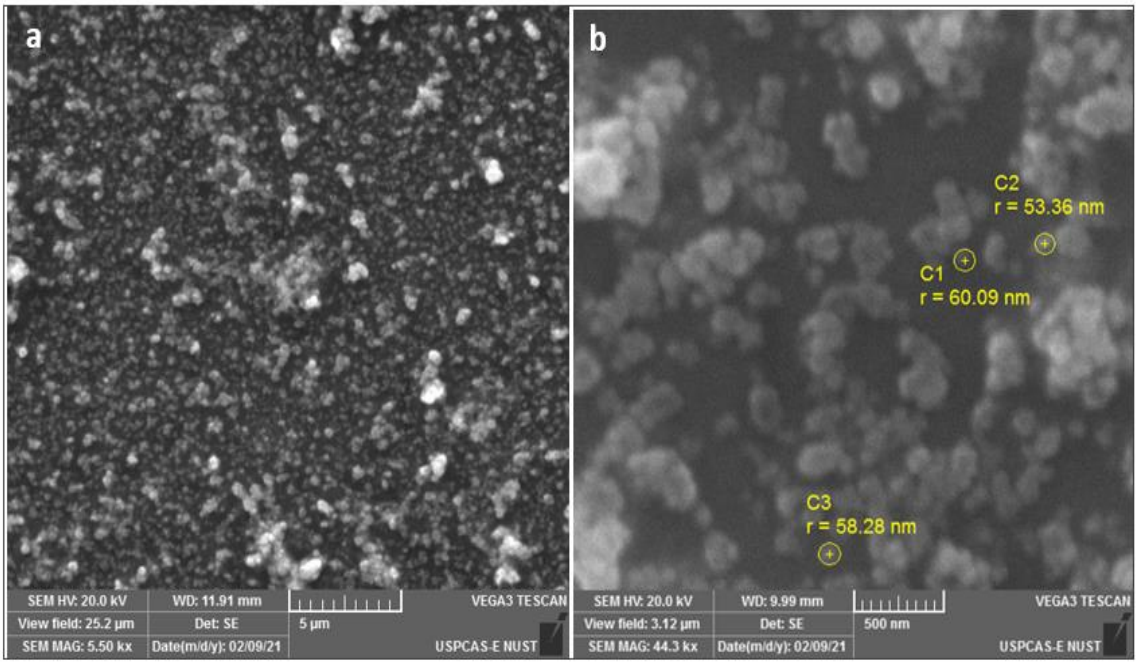

Figure 23 SEM results of (Au@Ag)20 at (a) 5 µm and (b) 500 nm, respectively.

Figure 23 illustrate SEM images of (Au@Ag)20 core-shell NPs produced, but small size spherical particles can also be noticed easily with average size of particle r =53.77 nm. In fig (a and b) the structure and morphology of (Au@Ag)20 core-shell nanostructure can be realized with the help of the scanning electron microscope and Au and Ag are in the ratio 5.34: 4.03% confirmed by EDS. All the SEM images displays uniform core shell NPs which also disclose the fact that as the quantity of Au seed increases then silver shell form and particles size decreases. Average size of particle is r=57.2 nm and r=53.77 nm for (Au@Ag)2 and (Au@Ag)20, respectively.

4.4 EDS

The elemental plotting of (Au@Ag) core-shell NPs by EDX are shown in *Figure 24* and *Figure 25*. The successful development of the bimetallic core-shell NPs is indicated by the variation of

Au and Ag quantity. ***Table 1*** and ***Table 2*** shows the EDS values (Au@Ag)2 and (Au@Ag)20 core-shell nanoparticles from two distinct points.

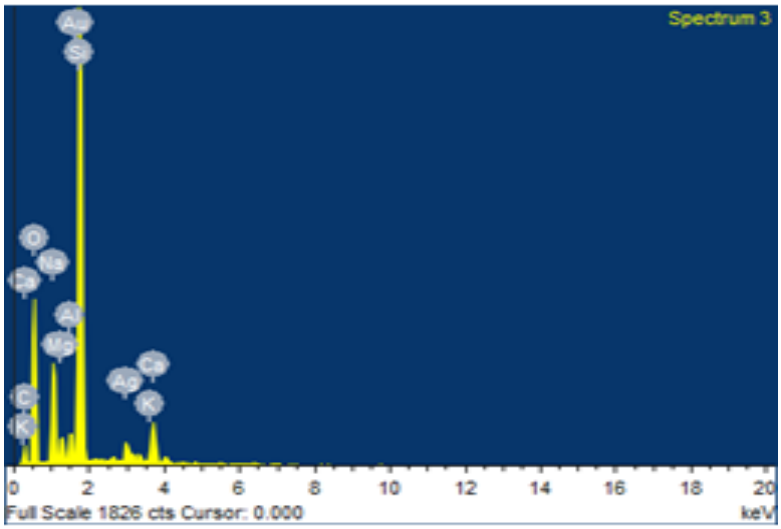

Figure 24 EDS spectrum of (Au@Ag)2 confirming the elements.

Table 1 Weight % and Atomic % of elements in (Au@Ag)2 for EDS.

Elements	**Weight%**	**Atomic%**
C K	13.01	20.42
O K	44.71	52.67
Na K	7.68	6.29
Mg K	1.32	1.02
Al K	1.32	0.92
Si K	23.87	16.02
K K	0.65	0.31
Ca K	3.61	1.70
Ag L	3.46	0.60
Au M	0.38	0.04
Totals	100.00	

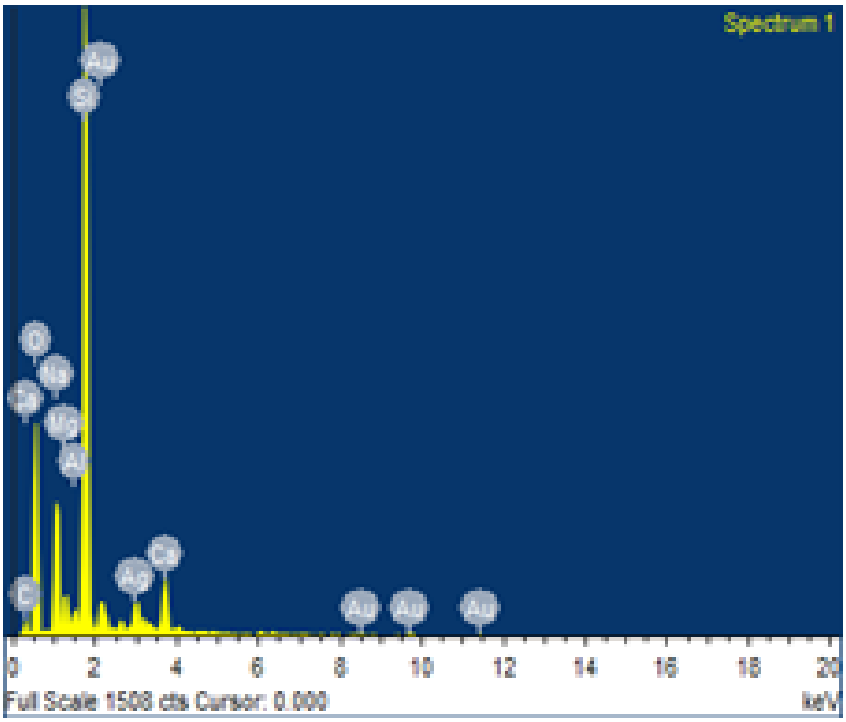

Figure 25: EDS spectrum of (Au@ Ag)20 confirming the elements.

Table 2 Weight % and Atomic % of elements in (Au@ Ag)20 for EDS.

Elements	Weight%	Atomic%
C K	7.72	13.21
O K	43.51	55.93
Na K	7.93	7.09
Mg K	1.59	1.35
Al K	0.63	0.48
Si K	25.56	18.72
Ca K	3.68	1.89
Ag L	4.03	0.77
Au M	5.34	0.56
Totals	100.00	

4.5 FTIR

FT-IR spectroscopy study of the AuNPs and (Au@Ag) nanoparticles show the availability of functional *Figure 26* indicates that characteristic core of AuNPs is changing from the core-shell

NPs, showing that different capping agent were involved for the core-shell NPs stabilization. The (Au@Ag)2 shows characteristic cures at 1512 cm^{-1} (C=O stretching in COO-), 1718cm^{-1} (C=C), 1973 (C=O) and a broad spectrum at 3741 cm^{-1} (H bounded OH stretching). Similarly (Au@Ag)20 shows characteristic cores at 1514 cm^{-1} (C=O asymmetric stretching in COO–), 1697cm-1 (C=C) and a broad spectrum at 3741 cm-1 (H bounded O_H stretching) which is the vibration of the carboxyl group (alcohols and phenols)) relates to functional groups that displays characteristic like citrate and ascorbic acid *Table 3.*

According to Womiloju, Aisha A., et al [52] the stretching and bending of peaks derived from sodium citrate and ascorbic acid that are accountable for both core shell NPs reduction and stabilization by reporting similar results. These wave numbers signal stretching and peaks vibrational bending.

AuNPs showed several peaks at 1510, 1697,1967,2165,2356, and 3623cm^{-1}. The peaks at 1510 and 1967 corresponds to COO^- and C=O group of primary hydroxyls Stretch Out which signifies the interaction stuck between citrate ions and AuNPs. Following table summarizes wavelengths and their corresponding functional groups.

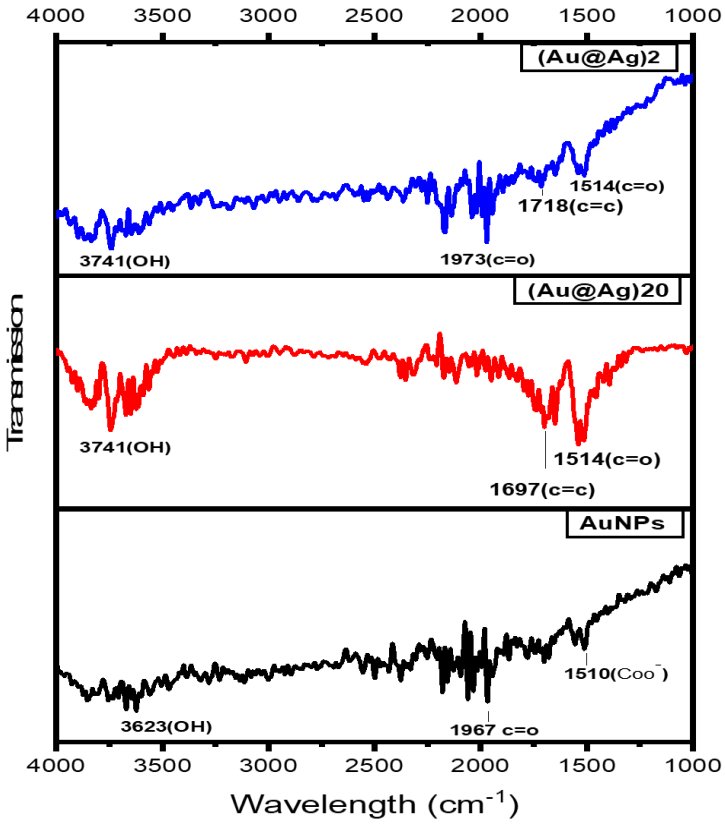

Figure 26 Comparison of FTIR spectra of AuNP (black), (Au@Ag) 20 core-shell NPs (red), (Au@Ag) 2 core-shell NPs (blue).

Table 3 Wavelengths and their corresponding functional groups.

Wave number (cm^{-1})	**Bond stretching**	**Functional groups availability**
3741	O-H stretch, H bonded	Carboxylic Acids (ascorbic acid)
3623	O-H bonded	Water
1967, 1514, 1973	C=O bonded	Carbonyl (trisodium citrate)
1697, 1718	C=C bonded	C=C double bound (ascorbic acid)
1510	Coo^- bonded	Carbonyls (trisodium citrate)

4.6 RAMAN Spectroscopy

To further study the effect of light on the sample RAMAN Spectroscopy was performed. It is a chemical fingerprint that gives frequent details about similarities and differences of the samples. *Figure 27* shows the SERS spectra of gold and (Au@Ag) core-shell bimetallic NPs containing changed sizes. AuNPs dropped on glass illustrate a very weak Raman spectrum indicate that AuNPs are a SERS-inactive substrate. While (Au@Ag) core-shell NPs monolayer displays a stronger and determined spectrum as compared to gold and silver NPs, this discloses the fact that these core-shell NPs are more powerful and a SERS-active substrate. These characteristic can be due to electronic ligand consequence in core-shell NPs and localized electric field enhancement [53].

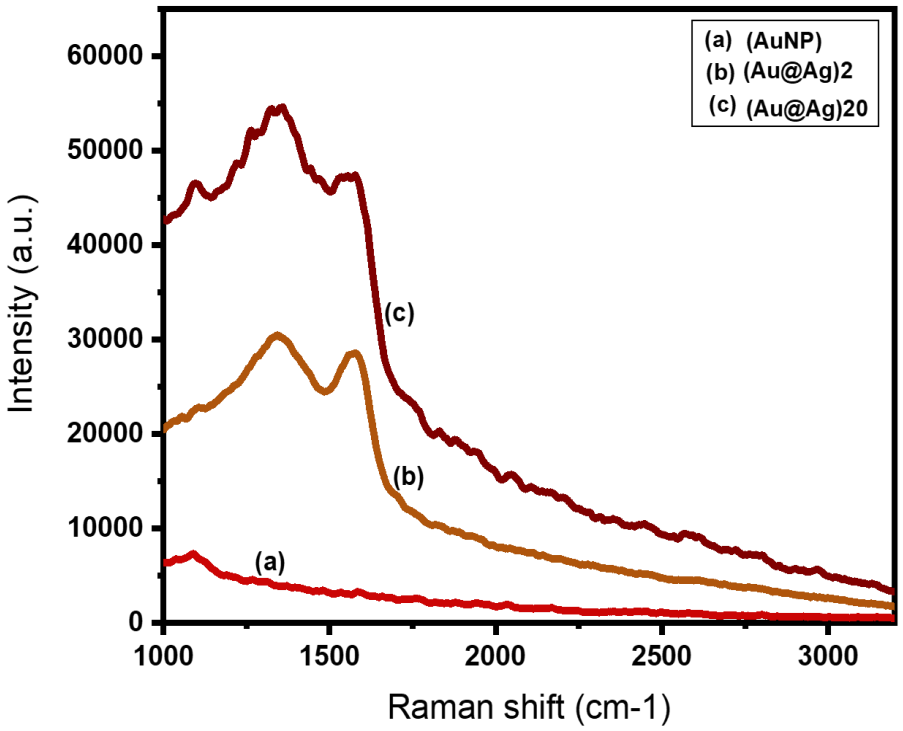

Figure 27: SERS of (a) AuNPs, (b)(Au@Ag)2 and (c)(Au@Ag)20.

The fermi level for Au is about -5.0 eV which is lower than the fermi level for Ag (-4.6 eV) due to which the Au atoms as a core material exhibit a strong electronic effect on the Ag atoms as a shell material by charge transfer. This in turn causes the silver atoms in shell more active as compared to pure Ag NPs. From the SERS spectrums it is evident that the particles with smaller size show more intense spectrum as compared to particles with large sizes. In other word we can summarize the results that with the increase in Au seed volume the particles sizes decreases and in turn SERS spectrum intensity become high.

4.7 Glucose Sensor

The electrochemical behavior of (Au@Ag) NPs was investigated from its redox behavior at modified GCE electrodes without using any binder. The sample coated GCE, platinum wire and Ag/AgCl were used as a working, counter, and reference electrodes, respectively. Additionally, the amperometric, sensitivity and selectivity responses toward the consecutive of addition of concentration of glucose was conducted in 0.1M sodium hydroxide solution at +0.6 and +0.75 potential.

4.7.1 CV

The cyclic voltammetry was directed at a scan rate of 20 mV s^{-1} for testing glucose concentration in (0.1 M) sodium hydroxide solution as displayed in *Figure 28.* This shows an inhibitory effect when the glucose concentration changes from 0.2-0.9 mM and 0.1-0.5 mM for (a) and (b) correspondingly where decrease in current occur.

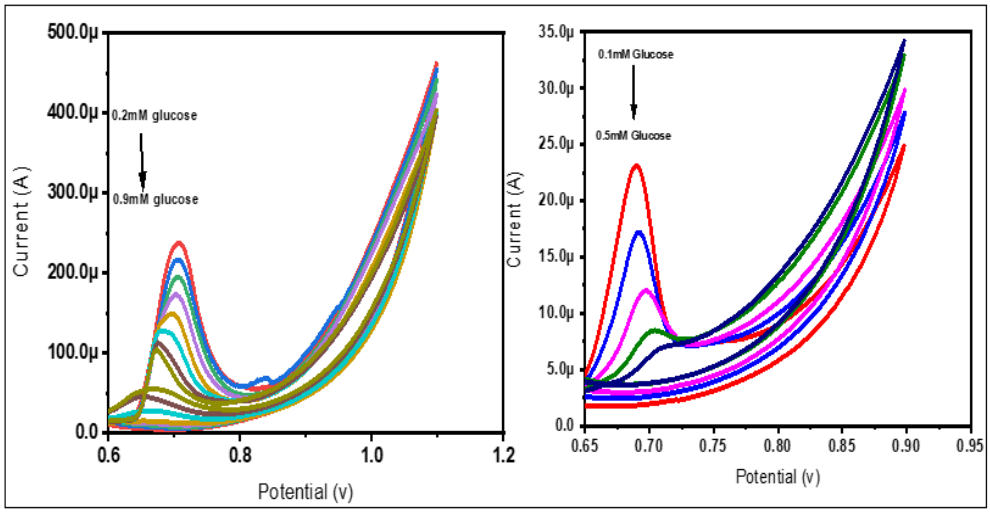

Figure 28 The CV response of a) (Au@Ag)2, b) (Au@Ag)20 in 0.1 M NaOH.

Figure 29 illustrate the effect of scan rate on the cyclic voltammetry (CV) of (Au@Ag)2 was conducted at 1mM glucose in (0.1 M) sodium hydroxide solution. This indicates that current increases with the increase in scan rate from 20-90 mVs^{-1}.

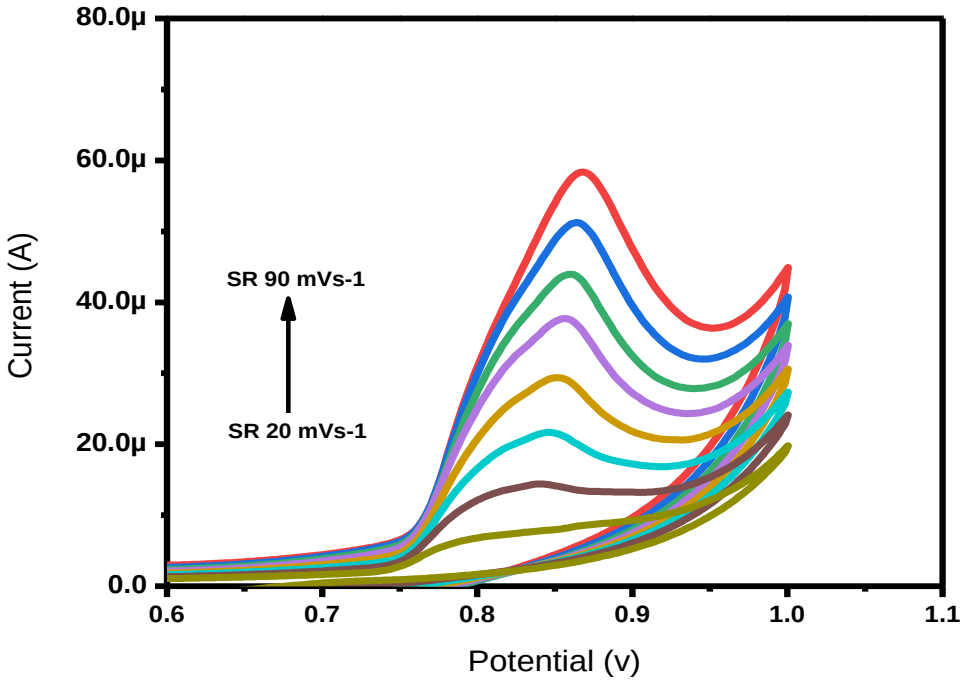

Figure 29: The CV response of (Au@Ag)2 with SR 20-90mVs^{-1}.

4.7.2 LSV

Figure 30 shows the Linear Sweep Voltammetry curves of Bare GCE in 0.1 M NaOH with and without 1 drop of sample. Further the figure shows the curves of GCE/(Au@Ag)2 and GCE/(Au@Ag)20 electrode in 0.1M sodium hydroxide in the lack of glucose.

Bare GCE shows no obvious current response in 0.1M sodium hydroxide even in the presence of glucose and a drop of core-shell sample at Scan rate 50mV/s. The oxidation peaks appear in case of both electrodes containing core-shell NPs. This indicates the superior conductivity of (Au@Ag) core-shell nanoparticles.

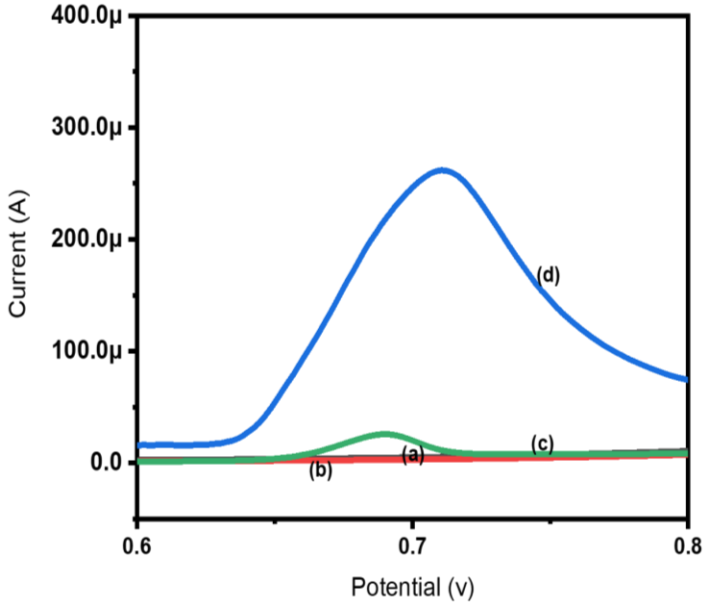

Figure 30 LSV in 0.1M NaOH solution, Scan rate 20mV/s a) Bare GCE with 0.1Mm glucose, b) Bare GCE with 0.1Mm glucose and a drop of /(Au@Ag)20 NPs, c) GCE/(Au@Ag)20 without glucose d) GCE/(Au@Ag)2 without glucose.

The LSV of (Au@Ag) core-shell NPs samples are displayed in *Figure 31* and *Figure 32*. With the addition of different glucose concentrations, the current of the anodic peak decreases with increase in glucose concentrations. This indicates an inhibitory effect of glucose on the electrochemical reactivity of the nano sensor.

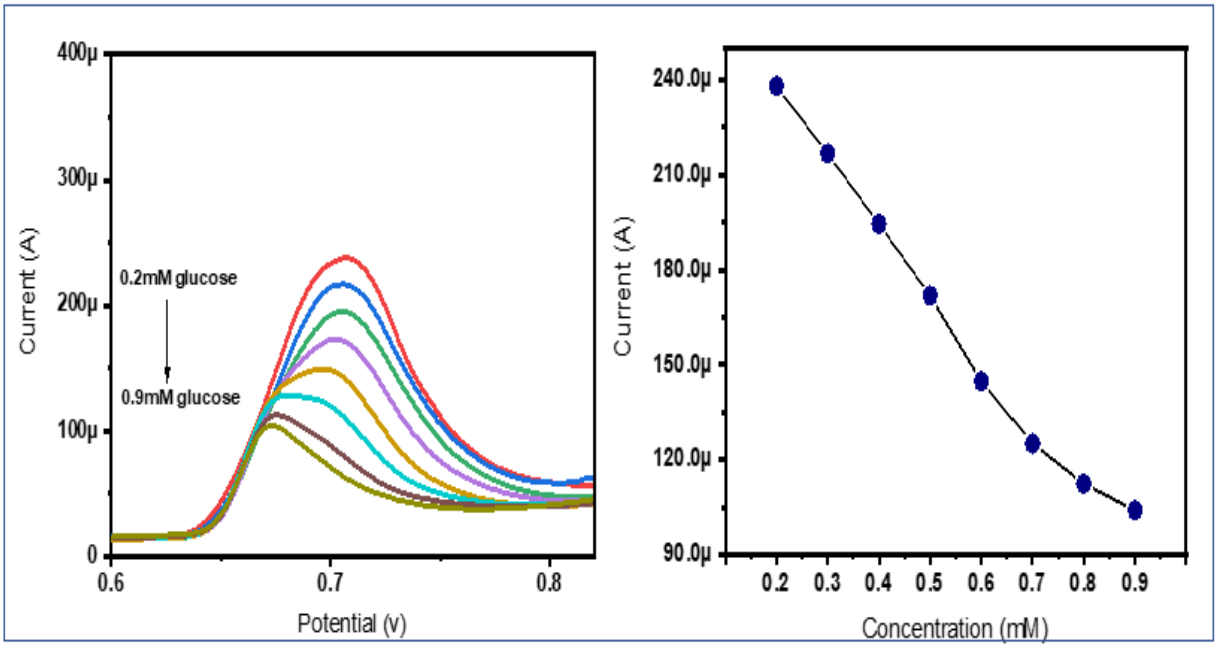

Figure 31 Linear sweep voltammogram recorded at different concentration of glucose at scan rate 20mV/s using a) (Au@Ag)2 core-shell electrode in 0.1mM NaOH solution from 0.2mM to 0.9 mM glucose b) The calibration curves of the biosensor.

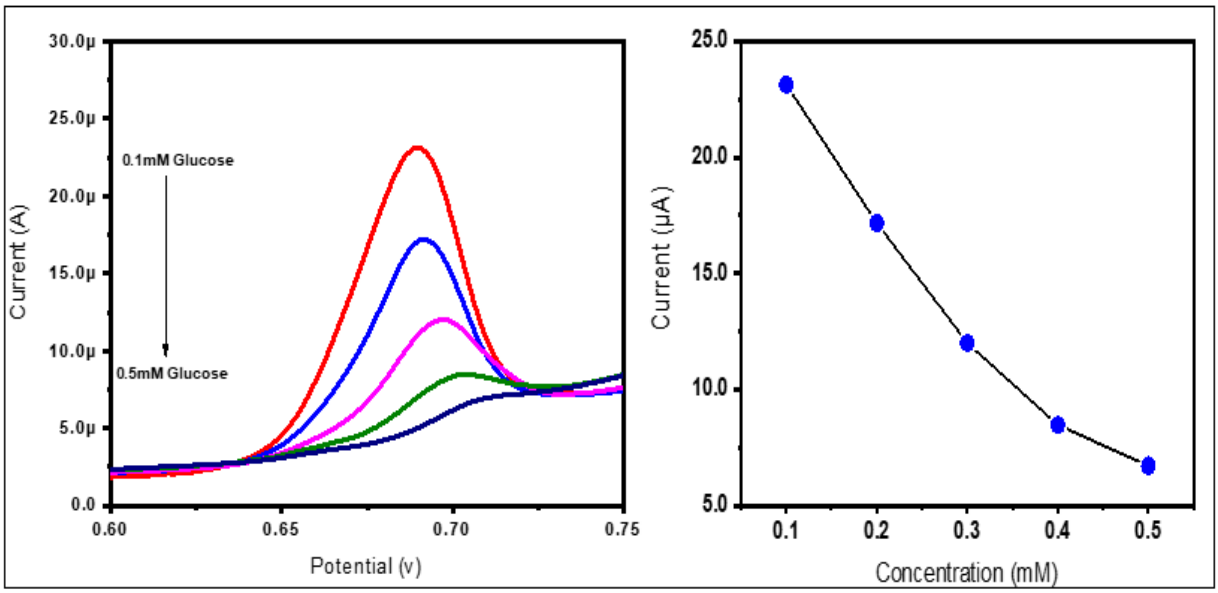

Figure 32 Linear sweep voltammogram recorded at different concentration of glucose at scan rate 20mV/s using a) (Au@Ag)20 core-shell electrode in 0.1mM NaOH solution with glucose concentration from 0.1-0.5mM, b) The calibration curve of the biosensor.

The electrochemical response of (Au@ Ag) core-shell NPs at the surface of electrode may represent the oxidation of Ag to Ag^{+2}. Higher potential than 0.36V is normally required to generate Ag^{2+}, hence we attribute the electrochemical signal here at higher than 0.36 V to correspond to the oxidation of Ag^{+} to Ag^{2+}, because the activation energy for the oxidation of Ag to Ag^{2+} decreases with decrease in interfacial energy and increase in surface- interface atoms portion. The glucose oxidation at working electrode surface is a simple process in which glucose first chemically attaches to AgNPs and then converted into gluconolactone with the emission of two electrons *Figure 33*.

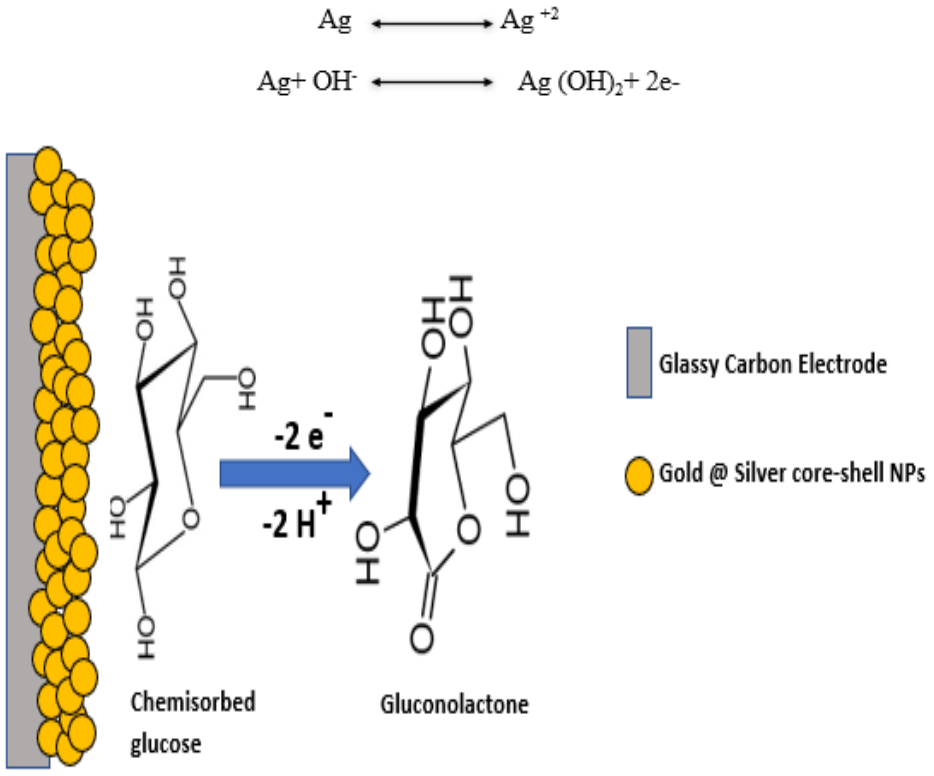

Figure 33 Schematic mechanism of glucose oxidation into gluconolactone at (Au@Ag) core-shell nanoparticles/GCE.

The current response with voltage in *Figure 31* is larger than *Figure 32* suggesting that the inhibitory effect increases with increase in core-shell NPs size conformed from SEM images. Scan rate is directly proportional to current, change in scan rate from 20 $mV\text{-}s^{-1}$ to 90 $mV\text{-}s^{-1}$ give increase in peak intensity and the background current. This occurs with a slight rise in peak potential as presented from LSV in *Figure 34*.

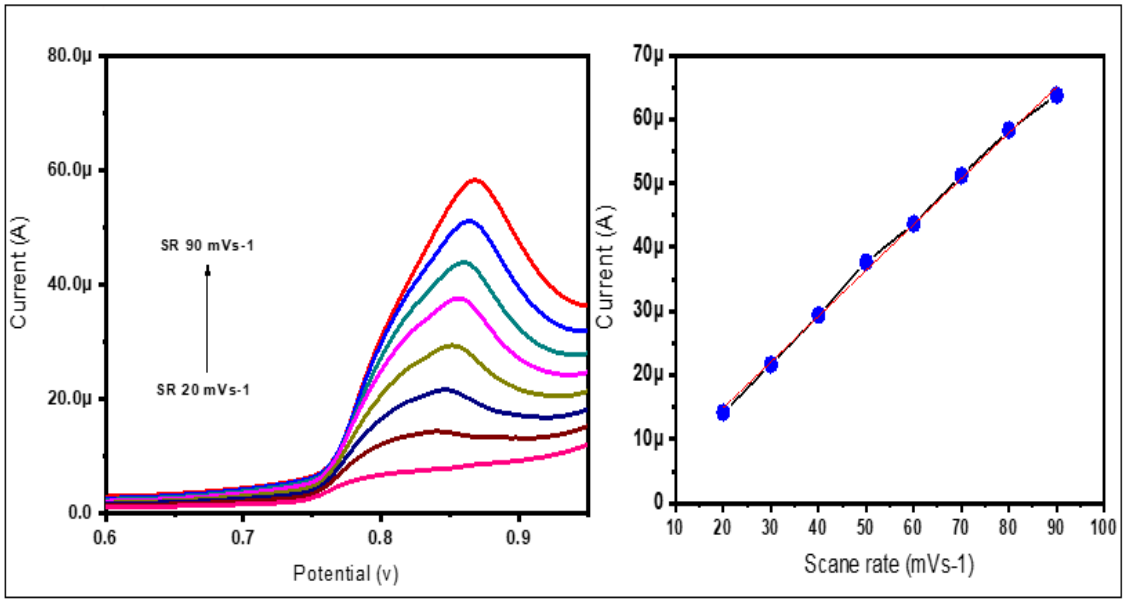

Figure 34 The response of biosensor with scan rate in the presence of 1mM glucose. a) LSV of (Au@ Ag)2 SR 20-90mVs-1 b) The calibration curves of the biosensor.

The improved linear range and limit of the detection for (Au@ Ag)2 core-shell nanoparticles for glucose sensing make it useful for quantitative use in electrochemical biosensors. The LOD was predicted to be 0.1 micromolar which is lower than the glucose concentration in sweat and saliva (8.3–120 micromolar) in healthy person [54]. Therefore, this nano sensor can be applied for noninvasive recognition of glucose in sweat and saliva.

4.7.3 Amperometric Performance of (Au@Ag)/GCE

Amperometric method was further conducted to examin the analytical performance of the glucose detection. The chronoamperometry, was implemented to examine the amperometric responses toward glucose oxidation due to its high detectivity, convective mass transportation and quick recognition. *Figure 35* and *Figure 36* show the typical amperometric responses of (Au@Ag)20/GCE and (Au@Ag)2/GCE on consecutive glucose addition into 0.1M sodium hydroxide solution stirring constantly. The diffusion rates of the reaction cab be described by linear range under varying glucose concentration. Above the saturation point i.e., 0.1mM glucose the sensor shows peculiar behavior that in case of low glucose concentration the oxidation products can inhabit the electrode surface less as compared to the high concentration of glucose. As a result,

high oxidation current occurred at low glucose concentration as compare relatively to the high glucose concentration. LOD was appraised to be 0.1 μM. Moreover, the performance of this biosensor is better as compared to other biosensors previously reported is shown in ***Table 4***. A comparison of (Au@Ag)20/GCE electrode with some other non-enzymatic sensor's sensitivity is shown below.

Table 4 Metal based non-enzymatic glucose sensors.

Electrode ingredients	**Linear range (mM)**	**Detection Limit (μM)**	**Sensitivity ($\mu A\ M^{-1}\ cm^{-2}$)**	**Supporting electrolyte**	**Ref**
Au nanowires	0.1–5	33	3700	0.1 M PBS, pH 7.2	[55]
Au@Ni	0.5-10	0.0157	23.17	0.1M NaOH	[56]
Au@NiCo	0.005-12	0.028	864.7	---	[57]
Au@ Pt	0.5–10.0 μM	445.7 (±10.3) nM	-------	0.5 M sulfuric acid (H_2SO_4)	[39]

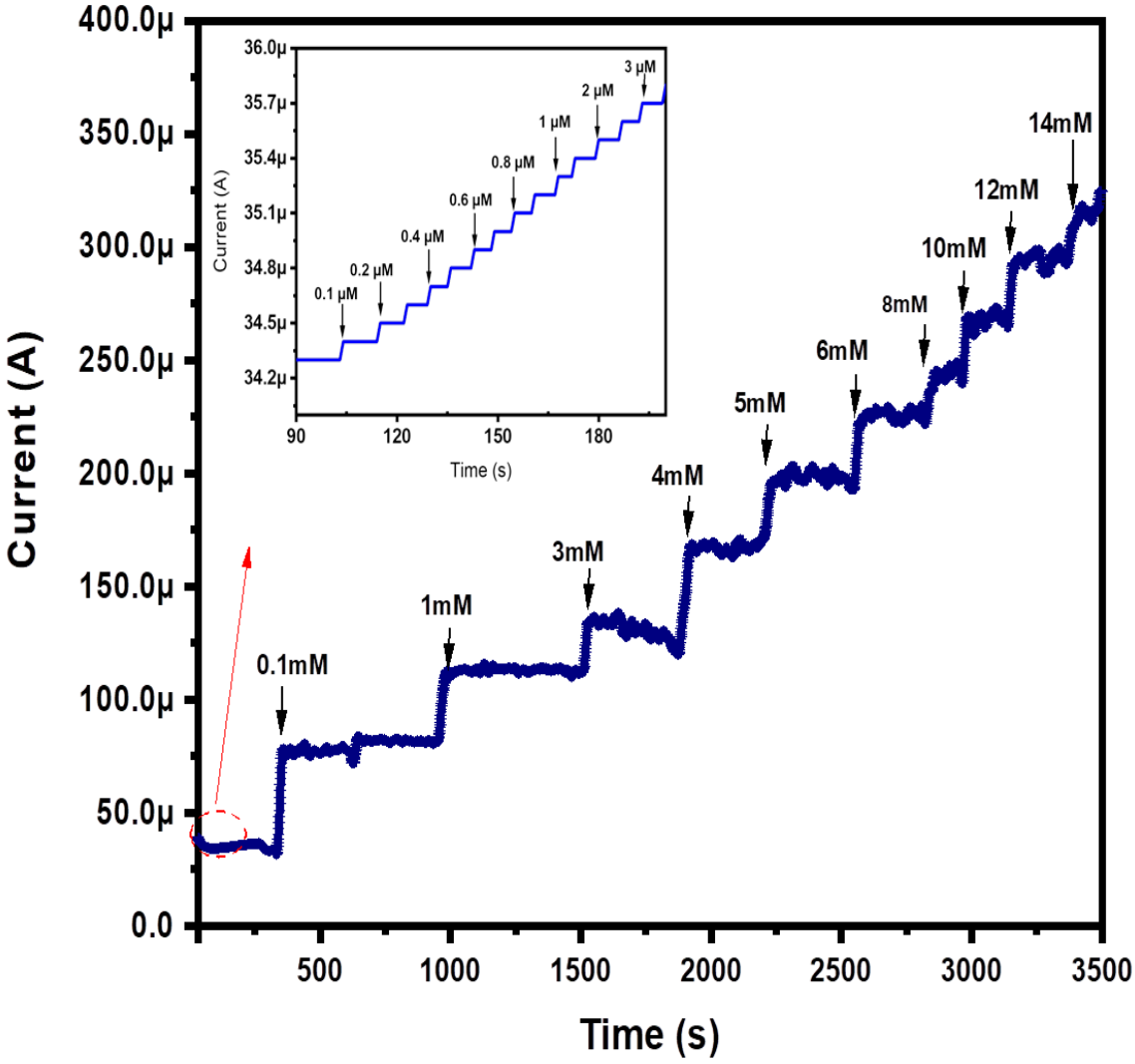

Figure 35 Chronoamperometric responses of (Au@Ag)20/GCE upon succeeding addition of glucose concentration (0.1-1Mm) at +0.6 V in o.1 M NaOH.

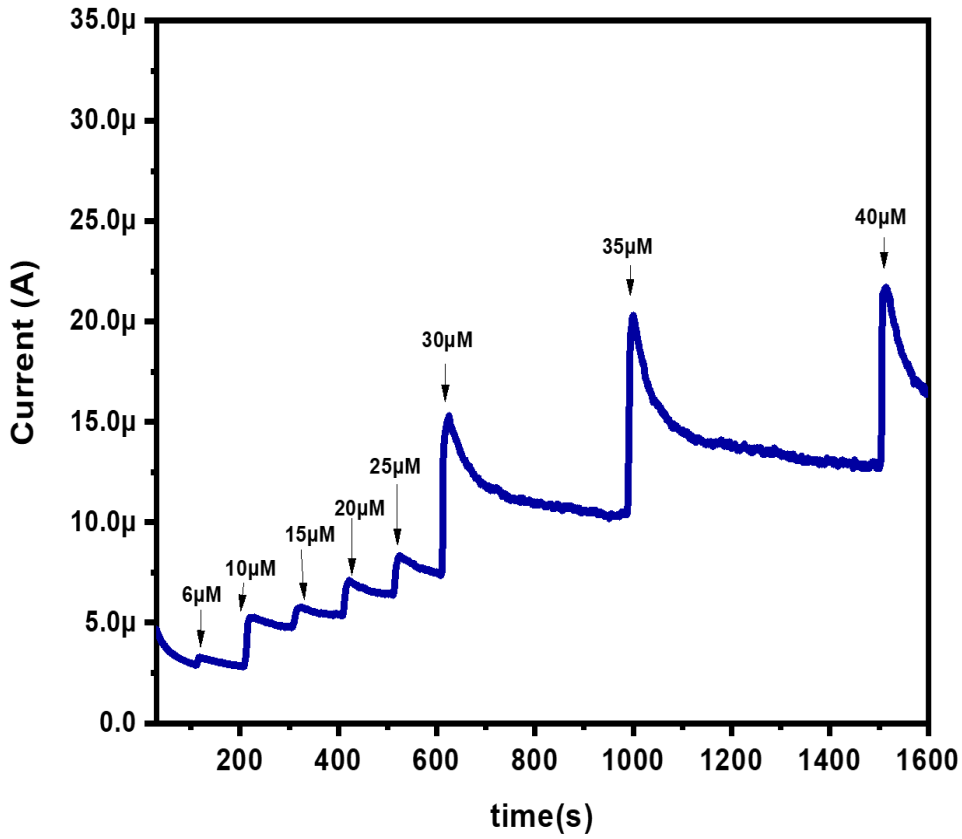

Figure 36 Chronoamperometric responses of (Au@Ag)2/GCE upon succeeding glucose concentration (6-40 μM) at +0.75V into 0.1 M NaOH.

4.7.4 Selectivity, Stability and Reproducibility of the Biosensor

The most important property of non-enzymatic sensors is to differentiate the capability toward interfering species [58]. Selectivity of prepared bimetallic core-shell NPs biosensor was evaluated by adding AA and UA as interfering substances commonly found in sweat and saliva and in blood. The biosensor shows no obvious response to these substances Figure 37 and *Figure 38* show high selectivity of the biosensor towards glucose detection.

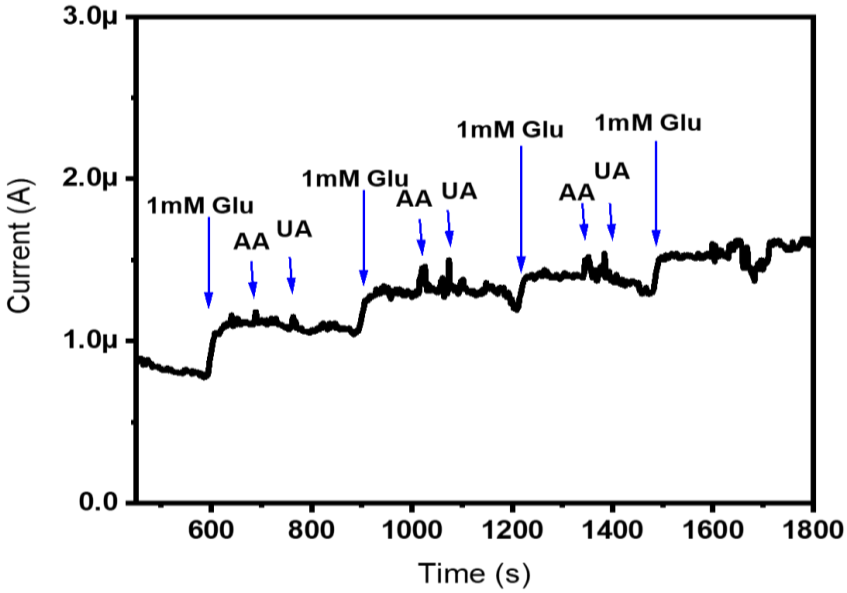

Figure 37:Selectivity of biosensor (Au@Ag)20 on successful addition of glucose and 50 micromolar ascorbic and 50 micromolar uric acid.

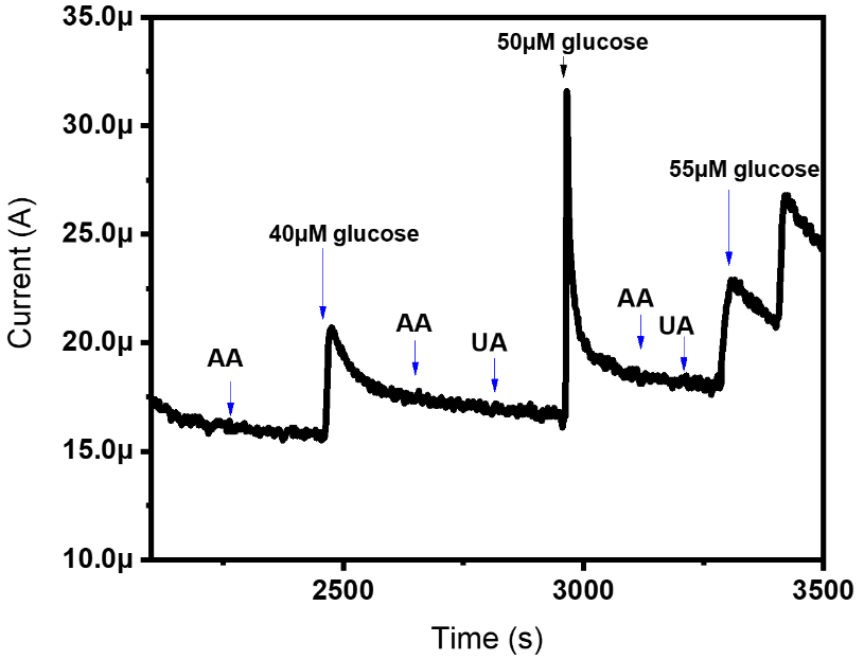

Figure 38: Selectivity of biosensor (Au@Ag)2 on successful addition of glucose and 50 micromolar ascorbic and 50 micromolar uric acid.

4.7.5 Stability of the Modified Sensor

The biosensor for stability was examined after 2 months from its amperometry response. The amperometric test was conducted at fixed potential (0.6V) in 0.1M NaOH. Current shows a linear response with glucose concentration as shown in *Figure 39,* indicating a good stability of the biosensor.

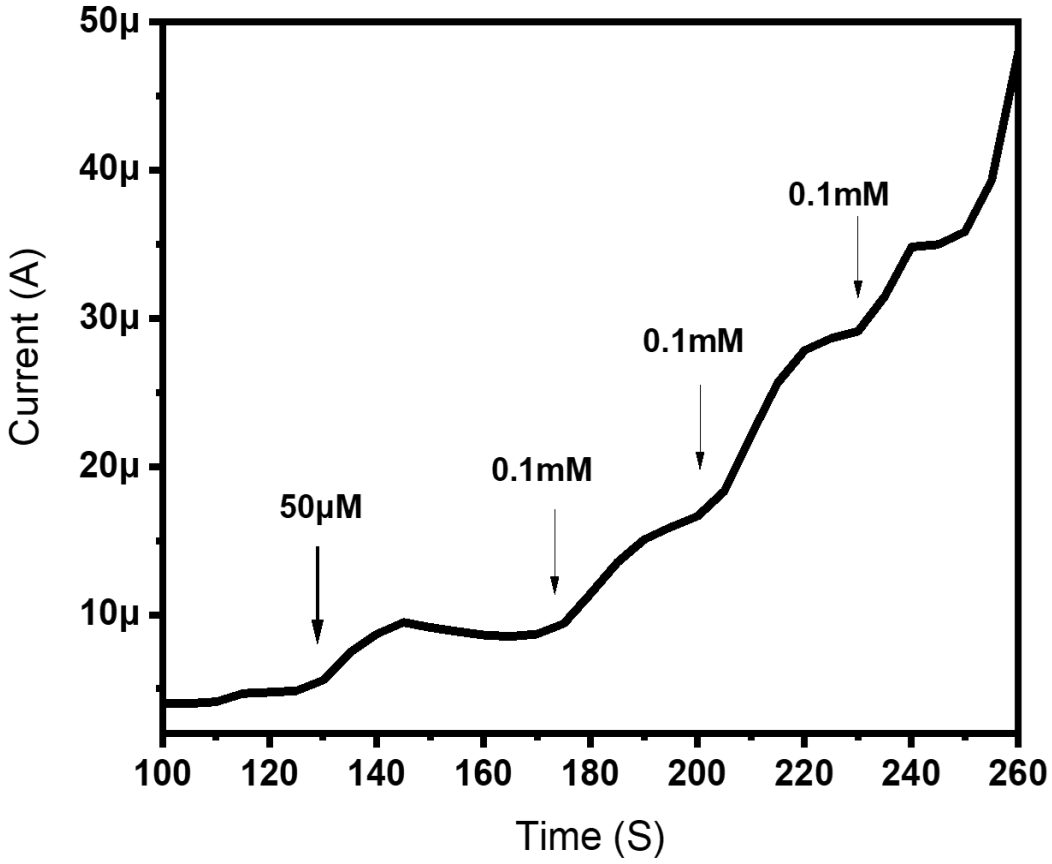

Figure 39 Stability of biosensor (Au@Ag)20 on successful addition of 50 micromolar 0.1Mm Glucose.

Chapter 5

Conclusion

The enzyme dependent and enzyme independent glucose sensors are well known but non-enzymatic glucose sensors based on (Au@ Ag) core-shell NPs shows excellent electrochemical response. From our best knowledge the application of non-enzymatic (Au@Ag) core-shell NPs in electrochemical sensing of glucose is not yet reported.

A non-enzymatic (Au@Ag) core-shell NPs based sensor for the detection of glucose in an alkaline medium (0.1M) sodium hydroxide solution was successfully developed using electrochemical measurements. XRD, FTIR, RAMAN and UV conformed (Au@Ag) core-shell NPs fabrication while the shape, size, and core-shell ratios of the (Au@Ag) core-shell NPs were confirmed by SEM and EDS analysis. The electrochemical response of the prepared biosensor was confirmed by Cyclic voltammetry. Chronoamperometry was also conducted which conformed that neither ascorbic acid nor uric acid interfered with the prepared glucose biosensor demonstrate that the selectivity of this sensor is admirable. The prepared NPs show constancy in water suspension for several months which indicate that no aggregations of nanoparticles occur. The (Au@Ag) core-shell NPs based non-enzymatic sensor demonstrated the superlative sensitivity for glucose sensing amongst the detectors evaluated. To employ the nano biosensor for real time glucose monitoring and in vivo upcoming studies will be required.

References

1. Hulla, J., et al., *Nanotechnology: History and future.* 2015. **34**(12): p. 1318-1321.
2. Feynman, R.P.J.R., *There's plenty of room at the bottom.* 2011. **16**(9): p. 890-905.
3. Li, X., *Applications for nanomaterials in critical technologies*. 2010, University of Illinois at Urbana-Champaign.
4. Fang, M., et al., *Degradation of nanoRNA is performed by multiple redundant RNases in Bacillus subtilis.* 2009. **37**(15): p. 5114-5125.
5. Di Guglielmo, C., et al., *Embryotoxicity of cobalt ferrite and gold nanoparticles: a first in vitro approach.* 2010. **30**(2): p. 271-276.
6. Saha, K., et al., *Gold nanoparticles in chemical and biological sensing.* 2012. **112**(5): p. 2739-2779.
7. Nayar, D., et al., *Relating structure, entropy, and energy of solvation of nanoscale solutes: Application to gold nanoparticle dispersions.* 2012. **116**(43): p. 13124-13132.
8. Trügler, A., et al., *Influence of surface roughness on the optical properties of plasmonic nanoparticles.* 2011. **83**(8): p. 081412.
9. Caro, C., et al., *Silver nanoparticles: sensing and imaging applications.* 2010: p. 201-223.
10. Li, D., A. Wieckowska, and I.J.A.C. Willner, *Optical analysis of Hg2+ ions by oligonucleotide–gold-nanoparticle hybrids and DNA-based machines.* 2008. **120**(21): p. 3991-3995.
11. He, S., et al., *Design of a gold nanoprobe for rapid and portable mercury detection with the naked eye.* 2008(40): p. 4885-4887.
12. Chen, Y., et al., *A dual-mode fluorometric/colorimetric sensor for Cu 2+ detection based on hybridized carbon dots and gold–silver core–shell nanoparticles.* 2019. **144**(14): p. 4250-4257.
13. Neuschmelting, V., et al., *Dual-modality surface-enhanced resonance Raman scattering and multispectral Optoacoustic tomography nanoparticle approach for brain tumor delineation.* 2018. **14**(23): p. 1800740.
14. Fabrega, J., et al., *Silver nanoparticles: behaviour and effects in the aquatic environment.* 2011. **37**(2): p. 517-531.
15. Zhang, X., et al., *Sensitive colorimetric detection of glucose and cholesterol by using Au@ Ag core–shell nanoparticles.* 2016. **6**(41): p. 35001-35007.
16. Jakab, A., et al., *Highly sensitive plasmonic silver nanorods.* 2011. **5**(9): p. 6880-6885.
17. Sztandera, K., M. Gorzkiewicz, and B.J.M.p. Klajnert-Maculewicz, *Gold nanoparticles in cancer treatment.* 2018. **16**(1): p. 1-23.
18. Wang, Z., et al., *Design of polymeric stabilizers for size-controlled synthesis of monodisperse gold nanoparticles in water.* 2007. **23**(2): p. 885-895.
19. Doria, G., et al., *Noble metal nanoparticles for biosensing applications.* 2012. **12**(2): p. 1657-1687.
20. Samal, A.K., et al., *Size Tunable Au@ Ag core–shell nanoparticles: synthesis and surface-enhanced raman scattering properties.* 2013. **29**(48): p. 15076-15082.
21. Yuan, P., et al., *Plasmon coupling-enhanced two-photon photoluminescence of Au@ Ag core–shell nanoparticles and applications in the nuclease assay.* 2015. **7**(22): p. 10233-10239.

22. Tan, C., et al., *A self-supporting bimetallic Au@ Pt core-shell nanoparticle electrocatalyst for the synergistic enhancement of methanol oxidation.* 2017. **7**(1): p. 1-10.
23. Henning, A.M., et al., *Gold–palladium core–shell nanocrystals with size and shape control optimized for catalytic performance.* 2013. **125**(5): p. 1517-1520.
24. Xu, W., et al., *An electrochemical aptasensor for thrombin using synergetic catalysis of enzyme and porous Au@ Pd core–shell nanostructures for signal amplification.* 2015. **64**: p. 423-428.
25. Selvakannan, P., et al., *Synthesis of aqueous Au core− Ag shell nanoparticles using tyrosine as a pH-dependent reducing agent and assembling phase-transferred silver nanoparticles at the air− water interface.* 2004. **20**(18): p. 7825-7836.
26. Tsuji, M., et al., *Role of chloride ions in the formation of Au@ Ag core–shell nanocrystal structures by using a microwave–polyol method.* 2008. **317**(1-3): p. 247-255.
27. Lu, L., et al., *Core–shell gold/silver nanoparticles: Synthesis and optical properties.* 2013. **392**: p. 90-95.
28. Yu, H., Y.J.S. He, and A.B. Chemical, *Seed-assisted synthesis of dendritic Au–Ag bimetallic nanoparticles with chemiluminescence activity and their application in glucose detection.* 2015. **209**: p. 877-882.
29. Ray, P.P.J.S.R., *Continuous glucose monitoring: a systematic review of sensor systems and prospects.* 2018.
30. Clark Jr, L.C. and C.J.A.o.t.N.Y.A.o.s. Lyons, *Electrode systems for continuous monitoring in cardiovascular surgery.* 1962. **102**(1): p. 29-45.
31. Zhang, H., W. Zhang, and A. Zhou, *Smartphone for glucose monitoring*, in *Smartphone Based Medical Diagnostics*. 2020, Elsevier. p. 45-65.
32. Wientjes, K.J.C., *Development of a glucose sensor for diabetic patients*. 2000: University Library Groningen][Host].
33. Krishnan, S.K., et al., *Chitosan-covered Pd@ Pt core–shell nanocubes for direct electron transfer in electrochemical enzymatic glucose biosensor.* 2017. **2**(5): p. 1896-1904.
34. Zhou, Y.-G., et al., *Gold nanoparticles integrated in a nanotube array for electrochemical detection of glucose.* 2009. **11**(1): p. 216-219.
35. Putzbach, W. and N.J.J.S. Ronkainen, *Immobilization techniques in the fabrication of nanomaterial-based electrochemical biosensors: A review.* 2013. **13**(4): p. 4811-4840.
36. Mei, H., et al., *Non-enzymatic sensing of glucose at neutral pH values using a glassy carbon electrode modified with carbon supported Co@ Pt core-shell nanoparticles.* 2015. **182**(11): p. 1869-1875.
37. Yang, X., et al., *A sensitive hydrogen peroxide and glucose biosensor based on gold/silver core–shell nanorods.* 2013. **108**: p. 39-44.
38. Chen, X., et al., *Nonenzymatic glucose sensor based on flower-shaped Au@ Pd core–shell nanoparticles–ionic liquids composite film modified glassy carbon electrodes.* 2010. **56**(2): p. 636-643.
39. Shim, K., et al., *Au decorated core-shell structured Au@ Pt for the glucose oxidation reaction.* 2019. **278**: p. 88-96.
40. Yang, Y., et al., *Preparation of Au–Ag, Ag–Au core–shell bimetallic nanoparticles for surface-enhanced Raman scattering.* 2008. **58**(10): p. 862-865.

41. Mohsin, M., et al., *An insight into the coating behavior of bimetallic silver and gold core-shell nanoparticles.* 2020. **15**: p. 1599-1612.
42. Darweesh, R.S., N.M. Ayoub, and S.J.I.j.o.n. Nazzal, *Gold nanoparticles and angiogenesis: Molecular mechanisms and biomedical applications.* 2019. **14**: p. 7643.
43. Skoog, D.A., F.J. Holler, and S.R. Crouch, *Principles of instrumental analysis*. 2017: Cengage learning.
44. Joshi, M., A. Bhattacharyya, and S.W. Ali, *Characterization techniques for nanotechnology applications in textiles.* 2008.
45. Smith, B.C., *Fundamentals of Fourier transform infrared spectroscopy*. 2011: CRC press.
46. Elgrishi, N., et al., *A practical beginner's guide to cyclic voltammetry.* 2018. **95**(2): p. 197-206.
47. Andrienko, D.J.J.W. and N.Y. Sons publication, *Cyclic voltammetry.* 2008: p. 3-12.
48. Haiss, W., et al., *Determination of size and concentration of gold nanoparticles from UV− Vis spectra.* 2007. **79**(11): p. 4215-4221.
49. Pande, S., et al., *Synthesis of normal and inverted gold− silver core− shell architectures in β-cyclodextrin and their applications in SERS.* 2007. **111**(29): p. 10806-10813.
50. Jana, N.R., L. Gearheart, and C.J.J.C.o.m. Murphy, *Evidence for seed-mediated nucleation in the chemical reduction of gold salts to gold nanoparticles.* 2001. **13**(7): p. 2313-2322.
51. Mandal, M., et al., *Synthesis of Au core–Ag shell type bimetallic nanoparticles for single molecule detection in solution by SERS method.* 2004. **6**(1): p. 53-61.
52. Womiloju, A.A., et al., *Microwave-Assisted Synthesis of Core–Shell Nanoparticles—Insights into the Growth of Different Geometries.* 2020. **37**(7): p. 2000019.
53. Kumar, G.P., et al., *Hot spots in Ag core− Au shell nanoparticles potent for surface-enhanced Raman scattering studies of biomolecules.* 2007. **111**(11): p. 4388-4392.
54. Yamaguchi, M., et al., *Noninvasively measuring blood glucose using saliva.* 1998. **17**(3): p. 59-63.
55. Nikolaev, K., et al., *Nonenzymatic determination of glucose on electrodes prepared by directed electrochemical nanowire assembly (DENA).* 2017. **72**(4): p. 371-374.
56. Gao, X., et al., *Core-shell gold-nickel nanostructures as highly selective and stable nonenzymatic glucose sensor for fermentation process.* 2020. **10**(1): p. 1-10.
57. Wang, L., et al., *Rattle-type Au@ NiCo LDH hollow core-shell nanostructures for nonenzymatic glucose sensing.* 2020. **858**: p. 113810.
58. Feng, D., et al., *Electrochemical glucose sensor based on one-step construction of gold nanoparticle–chitosan composite film.* 2009. **138**(2): p. 539-544.